UNIVERSIDADE DE LISBOA
FACULDADE DE CIÊNCIAS
DEPARTAMENTO DE BIOLOGIA VEGETAL

A STUDY ON THE GEOCHEMICAL CONDITIONS IN HYDROTHERMAL VENTS

Delfina Patrícia Henriques Pereira

Mestrado Bolonha em Biologia Molecular e Genética

Dissertação orientada por:
Dr. Prof. William F. Martin
Dr. Prof. Pedro João Neves e Silva

2020

I. Resumo

Assinaturas isotópicas de carbono sugerem que a vida na terra existe há mais de 3.95 Ga, mas pouco se sabe como e onde poderá ter surgido[1,2]. Na comunidade científica da Origem da Vida a via metabólica Acetil-coA desperta curiosidade pela sua simplicidade e origens longínquas. Esta via requer H_2 para fixar CO_2 e enzimas ricas em Ni e Fe nos seus centros catalíticos, para de forma exotérmica, produzir acetil-CoA tioéster como produto final[3,4]. A sua simplicidade permite que as reações possam ser replicadas no laboratório sem utilizar moléculas orgânicas. Varma et al. usou metais de valência zero e temperaturas entre os 30º–100 ºC para reduzir CO_2, a produtos intermédios da via acetil-coA, como acetato e piruvato[5]. Preiner et al. utilizou H_2 gasoso e com o auxilio de minerais férricos também conseguiu obter produtos desta via metabólica[6]. O sucesso destas experiências trouxe mais apoio para uma teoria altamente debatida de que a vida surgiu em fontes hidrotermais alcalinas no fundo do oceano. O exemplo mais mencionado destas estruturas é Lost City. As águas que circulam nesta fonte são altamente alcalinas (pH 9–11), com temperaturas moderadas (40–90 ºC) e ricas em H_2[7,8]. O processo de serpentinação que ocorre nestas estruturas sustenta uma fonte de hidrogénio molecular e calor constante[9], que contrastam com a àgua fria e acídica do oceano do Hadeano éon[10], criando gradientes de pH e temperatura nos poros das fontes hidrotermais[4]. Juntamente com os minerais untramáficos presentes nas suas paredes, que podem catalizar reações da via acetyl-coA[6], estas condições variadas atraem muita atenção dos cientistas que estudam a origem de biomoléculas e do primeiro metabolismo[11]. Contrariamente às suas propriedades químicas e geológicas, poucos testes experimentais existem sobre as propriedades físicas das fontes, nomeadamente a sua estrutura microporosa aberta. Alguns autores sugerem que os poros poderão ter sido importantes para favorecer a acumulação de produtos até concentrações suficientes para que um sistema autorreplicativo possa ter surgido[10,12] mas o trabalho de Yang et al. sugere contrariamente, que a sua estrutura aberta favorece o transporte de produtos, mantendo um constante estado de desequilíbrio[13]. Estruturas igualmente porosas, como argilas e aerogéis são altamente utilizados na indústria pelas suas capacidades de absorção, intercalação, propriedades de *swelling* e intercamadas altamente personalizáveis[14,15]. Zeolites são argilas de aluminossilicato de especial interesse industrial para catálise e para quando é necessária uma boa resistência hidrotérmica. A sua estrutura microporosa (< 1 nm) atribui-lhe uma área de superfície extensa com inúmeros centros ativos ácidos de *Lewis* e *Brønsted* mas também limita o transporte de produtos[16,17]. Consequentemente, zeolites hierárquicos são desenvolvidos artificialmente para promover a circulação de produtos pela estrutura, sem danificar as

propriedades catalíticas e de suporte catalítico destes minerais, combinando a sua estrutura microporosa com outra mesoporosa (2 – 50 nm)[17].

Para este trabalho foi desenvolvido um zeólito hierárquico com o propósito de replicar laboratorialmente a estrutura porosa das fontes hidrotermais e avaliar as vantagens e desvantagens catalíticas da mesma na redução de CO_2. Durante a composição do protocolo, foram testadas diferentes *Laponites* – argilas de silicato de magnésio sintéticas[18] – para averiguar a contaminação das mesmas com compostos orgânicos. Embora não tenha sido possível obter uma mistura sem qualquer contaminação, foi selecionada aquela em que foi detetada a menor quantidade de compostos orgânicos sem abdicar de uma estrutura porosa aberta, consistente e manuseável no laboratório (2.7 % Laponite-RD e 7.3 % zeolite (%w/w) em água pura; Figure 3.5.A, Appendix A. 1). A mistura de argilas foi colocada em tubos de vidro de 3 mL fechados e estes foram por sua vez colocados num reator de aço inoxidável onde foi realizado o trabalho experimental. Para comparar a eficiência com que este meio catalisa a redução de CO_2, também foram testadas amostras contendo apenas água, simulando um meio sem estrutura. Durante 16h, as amostras estiveram sob agitação a 70 ºC e 25 bar de H_2 e CO_2 (Table 2.2). Finalmente, os resultados foram avaliados por ressonância magnética nuclear de protões (RMN ^1H) e cromatografia líquida de alta eficiência (CLAE) para a deteção de etanol, metanol, acetato, formato e piruvato.

Os controlos efetuados revelaram que a contaminação é um problema mais extenso e profundo do que o antecipado. Não só o Laponite-RD apresentava contaminação, mas também foram detetadas contaminações nos utensílios utilizados ao longo do protocolo. Uma vez que a grandeza dos produtos nas amostras encontrava-se na escala nano e micro molar, mesmo após descontaminação dos materiais laboratoriais, era inevitável detetar contaminações vestigiais.

No entanto, foi possível observar de forma consistente o favorecimento da síntese de moléculas mais longas como acetato e piruvato no meio poroso, em vez de moléculas mais simples como o formato que foi detetado em quantidades mais significativas nas amostras com apenas água (Figure 3.7 Formate and acetate as a product of CO2 reduction compared between waterS, KOHS, and ZeoLapS. All samples had 15 bar of CO2 in addition to 10 bar of Ar or H2, to a total of 25 bar. In addition, samples could have magnetite (Fe3O4), nickel (Ni)). No contexto das fontes hidrotermais alcalinas, estes resultados sugerem que a sua estrutura geológica, não só poderá ter facilitado a catálise das primeiras moléculas orgânicas a partir de carbono e

hidrogénio abiótico, como poderá ter fornecido um meio onde a produção de moléculas mais complexas e com longas cadeias de carbono poderão ter sido favorecidas.

Consecutivamente, o segundo tópico deste trabalho reflete sobre o potencial redutor de hidrogénio abiótico e a estabilidade que as fontes hidrotermais poderão fornecer a moléculas orgânicas de maior complexidade, nomeadamente a dinucleótido de nicotinamida e adenina (NAD). Esta coenzima está presente no metabolismo de todos os organismos vivos e participa em inúmeras atividades metabólicas como a transferência de hidrogénio, sinalização, tem atividade transicional e participa como cofator em reações redox[19,20]. Na via acetil-coA participa juntamente com a ferridoxina na bifurcação de hidrogénio, um passo essencial para a ativação da molécula. Para o desenvolvimento do primeiro sistema catalítico autossustentável ter ocorrido nas fontes hidrotermais, moléculas antigas e essenciais para o metabolismo, como o NAD, teriam de ser estáveis e interagir com o meio eficientemente[21,22].

Para o efeito foram simuladas em laboratório várias condições hidrotermais com diferentes sais em solução e magnetita, um mineral presente nas fontes hidrotermais capaz de catalisar a redução de CO_2 a piruvato[5,6]. 3 mM de NAD em água pura ou em soluções salinas foram colocados em tubos de vidro de 1 mL num reator semelhante ao indicado anteriormente durante 2 h a 30 ºC, usando H_2 a diferentes pressões (2 bar e 10 bar) como a única fonte de hidrogénio para a redução de NAD^+ a NADH (Figure 1.3, Table 2.2). Uma vez que estes dois compostos têm espetros de absorvência distintos, os resultados foram obtidos por espectrofotometria e discutidos tendo em consideração controlos efetuados com Ar em vez de H_2.

Uma vez que as amostras não continham um sistema tampão nem um forte agente alcalino, tendiam para pHs acídicos após a adição de sais e durante o trabalho experimental com hidrogénio, o que poderá ter dificultado o favorecimento de reações de redução. No entanto, a 10 bar e na presença de magnetita, foi observado um grande aumento de absorvência do início para o fim da reação, no comprimento de onda correspondente a NADH (340 nm). Embora nenhuma amostra com sais em solução tenha apresentado resultados significantes, as amostras com ambos magnésio e magnetita tiveram o melhor resultado experimental deste projeto. Possivelmente o magnésio não é capaz de catalisar a redução de NAD^+ diretamente, mas poderá ter um papel importante na catálise realizada pela magnetita, ao facilitar a transferência do hidreto (Figure 3.1112). Finalmente, foi obtido o espetro total de amostras com NAD^+ e magnetita após a reação (30 ºC, 10 bar H_2, 2 h) onde é possível visualizar concretamente um pico a 340 nm, confirmando a síntese de NADH nestas condições.

Embora seja indispensável um esforço maior no desenvolvimento de protocolos livres de contaminações e com maior discriminação de produtos, este trabalho apresenta resultados concretos que sublinham a importância que as condições geoquímicas das fontes hidrotermais alcalinas poderão ter tido no desenvolvimento do primeiro sistema metabólico autocatalítico.

Palavras-chave: Fontes hidrotermais; estrutura microporosa; origem do metabolismo; redução; magnetite

II. Abstract

Alkaline hydrothermal vents are ancient ocean structures, H_2-producing, with pH, temperature and redox gradients which promote reduction and have been of great interest for Origin of Life researchers[10,23,24]. In the laboratory, CO_2 can be reduced under hydrothermal conditions to organic molecules, such as ethanol, formate, methane, acetate and pyruvate [255,6]. These molecules are also part of the ancient acetyl-CoA pathway, an exergonic, H_2-dependent, CO_2 reducing metabolic pathway, which possibly dates back to the Last Universal Common Ancestor (LUCA)[3,26]. In addition, the minerals within alkaline hydrothermal vents are rich in iron and nickel, two metals that are commonly found in the catalytic centers of modern-day enzymes, including the acetyl-CoA pathway[27]. They were also essential to catalyze CO_2 reduction to synthesize more complex molecules such as pyruvate in the laboratory[28,29]. The idea that alkaline hydrothermal vents can be associated to an ancient metabolic pathway leads to an interesting argument for the location of the origin of metabolism. In this work I looked to expand the range of studies with hydrothermal conditions to new topics beyond CO_2 reduction, exploring the effects of the complex microporous structure of these vents and if such rudimentary conditions could support modern day coenzymes and its redox reactions. For the first study an open microporous framework with zeolite and Laponite-RD was developed to simulate the vents' structure and reproduced previous CO_2 reduction experiments in this new setting. Secondly, the stability and reduction of nicotinamide adenine dinucleotide (NAD) under hydrothermal conditions was studied, an ancient coenzyme essential for metabolism.Results suggest that the framework used promotes the synthesis of more complex molecules such as pyruvate and acetate, in detriment of the production of simpler ones such as formate and that NAD is not only stable in alkaline fluids, but also can be reduced in the presence magnetite (Fe_3O_4). Reducing contamination and improving analytic methods are important next steps to take for this work, which already presents an avenue that further connects alkaline hydrothermal vents to the origin of metabolism.

Key words: Hydrothermal vents; microporous structure; origin of metabolism; reduction; magnetite

III. Index

IV. Table Index

V. Figure Index

1. Introduction

1.1 Origin of Metabolism and Hydrothermal vents

Life as we know it emerged from LUCA, an entity that shared the same genetic code and amino acid chirality, as all known living beings do, capable of proto-metabolism, compartmentalization, and inheritance[1]. The earliest living organism observed in the form of a fossil is 3.35 Ga, but carbon isotope signatures advocate for life being around for longer than 3.95 Ga[1,2]. How and where life could have emerged are topics of a vast debate on the Origin of Life (OoL) scientific community. Acetyl-CoA is a microbial, H_2-dependent CO_2 fixation pathway of great chemical simplicity and ancient roots, possibly dating back to LUCA[3,26]. It stands out for its exergonic properties, reducing CO_2 to a methyl group and CO, and through intermediate enzymatic nickel assisted reactions, it generates thioester acetyl-CoA as a final product[3,4]. Even though these reactions are enzymatically assisted, the catalysts are composed of native metals in their active sites, containing Fe, Ni, and other carbon-metal bonds[4,26,30]. Besides, the reactions are simple enough to occur spontaneously under a reducing environment, without the aid of enzymes[9,30]. Preiner et al. described it best, claiming that "the chemical reactions of the acetyl-CoA pathway themselves are older than the enzymes that catalyze them"[9]. However, in the absence of organic catalysts, for H_2-dependent CO_2 reduction to be at the origin of biochemistry, it needs an H_2 source and means for molecular hydrogen activation[30]. In the absence of a structured cell and a structured metabolism, these demands needed to be answered by the geochemical conditions surrounding such a primitive chemical system. That is at the bottom of the sea in alkaline hydrothermal vents, a highly discussed and supported theory for where the origin of life occurred. The best example is Lost City, a strongly alkaline hydrothermal vent (pH 9–11) rich in H_2 from olivine serpentinization and reduced warm water with temperatures ranging from 40–90 ºC[7,8]. Structures like this are exceptionally well preserved since the Hadean eon, and the conditions observed nowadays are most likely a good indicator of how these vents worked millions of years ago[31] There, cold water travels deep into cracks in the ocean's crust, and it heats up to 200ºC as it reacts with ultramafic rocks (high Fe^{2+} and Mg^{2+} and low silicate content) present in the lithosphere, bringing its products in the current that resurges warm alkaline fluids from the vents[25]. This exergonic reaction synthesizes mostly mafic minerals, but others can be produced: magnetite (Fe_3O_4), a typical product of serpentinization, hydrogen (H_2 and OH^-) produced as a result of Fe(II) minerals oxidation gives the vents their alkaline properties, methane (CH_4) and other low-molecular-mass hydrocarbons.

This convective current can also carry intermediate products, ions (Mg^{2+}, Fe^{2+}, Fe^{3+}, HS^-, HCO_3^-, etc.) and other molecules depending on the vent's mineralogy, that add to the complexity of these vents[4,9,24,25]. Contrastingly, during the Hadean, the ocean was twice as deep[32], its water was incredibly rich in CO_2, due to intense volcanic activity, and accordingly acidulous (pH 5–6)[10,11].As the warm alkaline fluid rises, it contacts cold, acidulous ocean water, resulting in carbonate precipitation[13,25]. This leads to the synthesis of precipitation membranes, which, together with water erosion and hydroxylation of the crust's minerals, constitute the vent's walls and complex network of open micropores (< 2 nm)[7,8,31]. In these interconnected pores, water from the crust and the sea interact to form pH and temperature gradients[4], further promoting a strong redox gradient that favors spontaneous CO_2 reduction in a H_2-rich system with temperatures that integrate the biologically relevant temperature range (0–120 ºC), making these vents an attractive possible location for the origin of metabolism[11]. These vents are also rich in native metals such as iron and nickel, which have been proved to catalyze acetyl-CoA reactions efficiently[28,29]. In this pathway, hydrogenases require iron in their active sites to activate hydrogen toprovide an electron source, and contain iron in their active sites[27,33]. Nickel, as mentioned before, is deeply involved in the intermediate steps of acetyl-CoA, being preserved within the active site of a central enzyme in CO_2 reduction – carbon monoxide dehydrogenase (CODH)[27,34]. Varma et al. used zero-valent metals involved in this pathway to reduce CO_2 at temperatures between 30–100 ºC and all showed to catalyze acetate production and other simpler molecules (10–200 µM of reduced carbon compounds). Fe^0, $Ni^{0,}$ and Co^0 also promoted the synthesis of pyruvate up to ~0.1 mM[5]. Preiner et al. tested if minerals frequently found in hydrothermal vents, which contain native metals, could catalyze CO_2 reduction with hydrogen gas as the electron source (instead of metals). Greigite (Fe_3S_4), magnetite, and awaruite (Ni_3Fe) all catalyzed the synthesis of formate, acetate, methanol, and pyruvate under hydrothermal vent conditions[6]. Such studies such can help to understand how a biochemical system could have arisen. Most experiments focus singularly on a variety of hydrothermal conditions and how these can impact biosynthesis. Even though the geological environment and location are heavily debated, few experimental tackle how these settings could affect biosynthesis, in laboratory conditions.

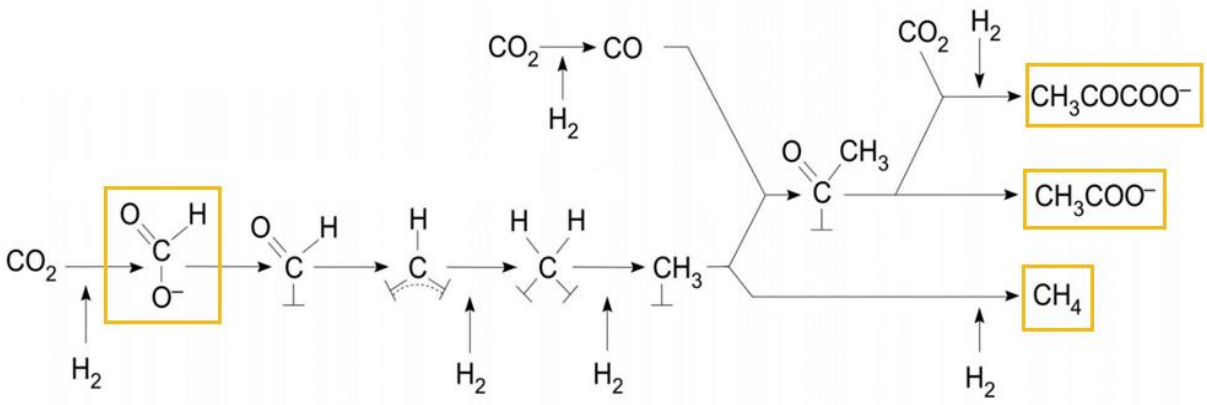

Figure 1.1 The chemical reactions of the linear acetyl-CoA pathway described by Fuch et al.[3]. Later it was found by Wagner et al.[35] that free formate is formed in the methanogen pathway and edited by Preiner et al.[6]. The "⊥" sign represents protein cofactors bound to carbon groups by nitrogen, cobalt, nickel, or sulfur atoms. In yellow boxes are highlighted formate, methane, acetate, and pyruvate, which were products obtained from CO_2 reduction using iron mineral catalysts in laboratory conditions[5,6].

One argument for the geological characteristics of alkaline hydrothermal vents as sites for the origin of life aretheir open porous structures. They have been described as a solution for product accumulation, possibly leading to sufficiently high concentrations for a self-replicating system to arise[10,12]. On the other hand, Yang et al. experimented on the "leakiness" of hydrothermal vents' structures, finding it promoted enhanced transportation, sustaining disequilibrium across sections of the vents[13]. Ultimately, alkaline hydrothermal vents stand out not only for their unique chemical properties but also fortheir geological composition and structure in assisting the origin of a proto-metabolism. Nonetheless, researchers frequently limit experiments to either one of the two properties when applied to CO_2 reduction. Replicating the alkaline hydrothermal vents' conditions, both morphological and chemical aspects could lead to a clearer picture of these deep oceanic structures' role in the origin of biochemistry. Therefore, this thesis presents a study on the effect of different media, structured and unstructured, on reducing both abiotic (CO_2) and biotic (NAD^+) compounds under alkaline hydrothermal vent conditions.

1.2 ZeoLap experiments

Replicating the complex system of interconnected micropores with a variety of gradients and minerals can be challenging. Herschy et al. attempted to do this by building a benchtop reactor with foam ceramics. While it stands out for engendering a complex system with precipitation chambers and two fluids that generated a pH gradient, it was also limited to mild hydrothermal conditions and ambient pressure[36]. The use of a foam ceramics to obtain a microporous structure

however, can be further explored. Ceramics are part of a broader group of clay minerals, notable for their absorption, intercalation, swelling properties, and changeable interlayers[14,15]. The interlayers constitute two sublayers of tetrahedral and octahedral sheets, in which chemical composition can be extensively tuned for the better interest of the developer[37,38]. Thus, not only can clays be found in nature, but a growing interest in their catalytic value for the industry, has dramatically expanded the library of these layered materials[39].

Zeolites are microporous clay minerals with extended surface area, excellent hydrothermal stability, Lewis and Brønsted acids as active sites, and shape selectivity, which makes these clays great catalysts and catalyst supports[16]. This aluminosilicate's microporous framework (typical pore size < 1 nm) also constitutes its most significant limitation, leading to slow reagent and product transfers to the active sites and formation of deposits that can affect production rates. Contrarily, mesoporous (2 – 50 nm) materials allow an excellent mass transfer but lack active sites and hydrothermal stability[17,40]. Hierarchical zeolites are the industry's answer to this problem, adding meso- and/or macropores (> 50 nm) to zeolites' structure. Even though they still contain fewer acid sites than standard zeolites, the enhanced circulation of mass provided by the larger pores increases the efficiency of each site[17,41]. Consequently, hierarchical zeolites have great mass diffusion without abandoning other advantageous properties of the usual microporous framework.

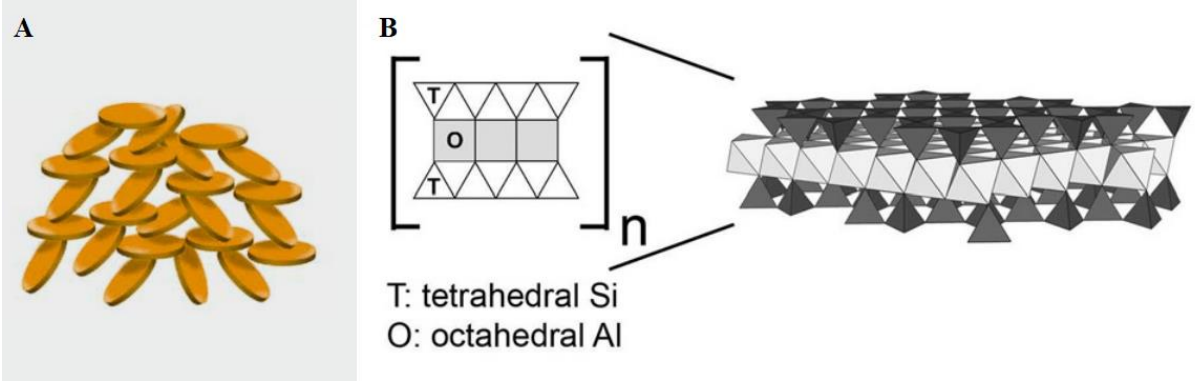

Figure 1.2 Schematic illustration of Laponite's and zeolite's molecular structure; A) Laponite's gel formation-house of cards structure, made by the suppliers[18]; B) Selvam's et al. take on the structure of clay minerals[42].

Referring to the problems and limitations encountered in replicating the hydrothermal vent conditions mentioned before, the next step for bottom-up approaches could be hierarchical zeolites. Both alkaline hydrothermal vents and hierarchical zeolites have a complex microporous structure, good mass flow, and metal-silicate based compositions. In the laboratory, hierarchical zeolites could reproduce the geochemical conditions in the vents and

unlock the possibility for more detailed studies on CO_2 reduction. Thus, for this work, a mixture of the two-layered silicates was developed to obtain a hierarchical zeolite: Laponite and zeolite, to which we called "ZeoLap". Laponite is a synthetic clay mineral, manufactured mainly as a rheology modifier and film former[18]. Its crystals are disk-shaped magnesium silicates with hydrated sodium ions that, through electrostatic forces, arrange in a "house of cards" structure. These small particles (25 nm wide and 0.92 nm tall) form a thixotropic gel stable at a wide range of temperatures, pH, and pressures[43,44]. Thus, it functions as a rheological additive to control matter flow even in harsh conditions. In theory, zeolite's ordered microporous structure with Laponite's "house of cards" structure could combine to generate a new complex porous framework, resistant to a diverse set of hydrothermal conditions and with excellent catalytic properties. Upon obtaining a mixture that maintained a stable gel-like structure under hydrothermal vents conditions, more tests were performed to finally access the problem proposed: how does the geochemical structure observed in hydrothermal vents affect CO_2 reduction? For this purpose, ZeoLap and ultra-pure water were used as a framework and frameless templates, respectively, for CO_2 reduction under hydrothermal conditions (70 ºC, 25 bar of CO_2, and H_2). The catalytic properties of nickel and iron were further explored by testing additional samples with Ni nano-powder and magnetite separately. Controls were performed in a CO_2-free environment, where the synthesis of organic compounds should not occur. The samples were analyzed via nuclear magnetic resonance (^{1}H-NMR) and high-performance liquid chromatography (HPLC) to detect the synthesis of formate, ethanol, acetate, methanol, and pyruvate, organic molecules already detected in previous similar studies after CO_2 reduction[6].

1.3 NAD experiments

So far in this work, simple reactions from the acetyl-CoA linear pathway were discussed, conditioned by far from equilibrium conditions provided inside the vents. But it is also essential to study if such setting could have supported the inevitable transition to a more complex and self-structured system. In this environment, minerals and native metals could have represented the first driving forces for geochemical reactions to be more complex and ordered. As mentioned before, the majority of the acetyl-CoA pathway enzymes are abounding of transition metals in their catalytic centers[34,45]. Thus, as it has been the norm for evolution, it is possible thatminerals were continuously preserved and merged with peptides to become protein active sites or cofactors[46]. The early involvement of electron carriers has been mainly discussed in the context of hydrothermal vents for electron bifurcation[26] – an endergonic redox reaction coupled

to an exergonic redox reaction as an energy-conserving mechanism[47]. As already pointed out earlier, hydrogenases are employing this process. Thereby electron carrier cofactors are involved both as electron donors and acceptors. Within anaerobes with necessary iron supplies, ferredoxins are the electron acceptors more frequently found[48]. This iron-sulfur protein is the most stable reducing molecule found in the cell, competing with nicotinamide adenine dinucleotide (NAD) for their ancient roots[49].

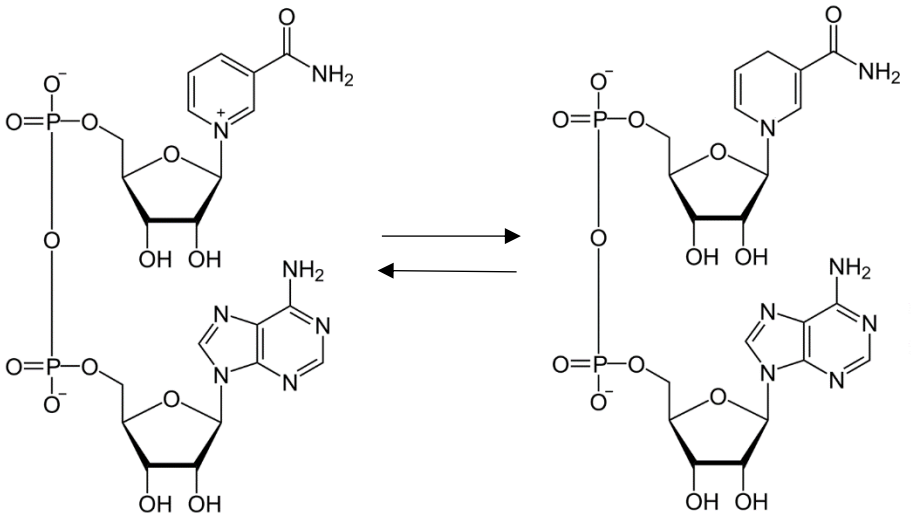

Figure 1.3 Nicotinamide adenine dinucleotide's structure was discovered by the Nobel Prize Laureates Arthur Harden and Hans von Euler-Chelpin of 1929 while studying sugar's fermentation. Otto Warburg later discovered the coenzyme role in hydrogen transfer in 1936[19].

NAD is an hydrogen carrier present in every organism and is composed of two mononucleotides: adenosine monophosphate (AMP) and nicotinamide mononucleotide (NMN). It is capable of hydrogen-transfer, several signaling events, transcriptional activity, participates as a cofactor in redox reactions, and others. Besides, many enzymes are NAD-dependent, predominantly hydrogenases[19,20]. NAD can be involved in electron bifurcation, both as hydrogen acceptor and donor, and its oxidation is often coupled to ferredoxin's reduction[48]. In alkaline hydrothermal vents, hydrogen donors for electron bifurcation could have represented the first step for a self-sustaining autocatalytic system, balancing the far from equilibrium conditions that stand far on the side of reduction. Whereas their role in hydrothermal vents is up for debate, their roles in ancient metabolic networks are not. In the last two decades, ferredoxin and NAD have been found to be essential elements of methanogens and acetogens' electron bifurcation and the acetyl-CoA pathway[21,22,50]. Certainly, for life to have had emerged in these vents, it would depend on electron bifurcation, thus such conditions would have to support molecules like ferredoxin and NAD, in a stable and functional manner,

for the development of a proto-metabolism. In addition, because the serpentenizing system of hydrothermal vents comprise an important hydrogen and energy source for CO_2 reduction, it is also important to ascertain if this abiotic source of hydrogen can also reduce more complex molecules such as NAD. While ferredoxin's iron-sulfur composition has been compared to that of hydrothermal vents' minerals, iron sulfides are capable of electron transfer and not hydride transfer. NAD's correlation to this environment has never been experimentally tested[51,52]. If this coenzyme was stable under such conditions while also effectively functioning as an hydride acceptor from abiotic H_2, it could represent an important transition point in the development of an autocatalytic system and would mean that these vents can support more complex organic molecules. Some studies have addressed NAD's stability under a comprehensive range of pH (~2 – ~8) and temperatures (15 ºC – 100 ºC)[53–56]. However, to date, there are no studies regarding NAD stability under vastly alkaline media, such as one of the alkaline hydrothermal vents. Thus, in this work it was studied the stability of NAD in mild hydrothermal conditions (30 ºC and 2/10 bar H_2), in its oxidized state (NAD^+), and if such reducing and austere environment would convert the molecule to its reduced state (NADH). As NAD reduction is often coupled with another compound's oxidation and requires an electron donor, we tested this hypothesis in different solutions, with either biologically relevant salts (NaCl and $MgCl_2$) or ferrous compounds (Cl_2Fe, $FeCl_3$, and Fe_3O_4) under the same conditions as mentioned above. NAD's reduced and oxidized forms present different photometric spectrums, with the first one presenting absorption peaks at 260 nm and 340 nm and the other only at 260nm[53]. Consequently, it was possible to compare NAD's spectra under different conditions and time points to address its stability and redox state, by verifying the presence of a peak at 340 nm through spectrophotometric analysis.

2. Methods and Materials

2.1 Laponite-RD and Zeolite Clay (ZeoLap)

2.1.1 ZeoLap Preparation

A protocol was developed for ZeoLap preparation. 10 mL of the ZeoLap solution was prepared in order to have three replicates for each sample. A glass beaker with a polytetrafluoroethylene (PTFE)-coated magnetic stirrer was used to prepare the mixture. 230 mg of Laponite-RD (BYK chemicals, Wesel, Germany) and 730 mg of Zeolite (Sigma-Aldrich, Steinheim, Germany) were added, composing about 10 % (w/w) of the final solution (Appendix A. 1). After placing the glass beaker on a stirring plate (400 rpm; Arex heating magnetic stirrer, VELP Scientifica, Usmate Velate (MB), Italy), 9 mL of ultra-pure water (pH 8,8; HPLC-grade, Fisher chemicals, Loughborough, UK) was gradually added to the mix. The beaker was sealed with aluminum foil to avoid significant water loss by evaporation and left mixing for 1 h, the necessary time to attain a homogenous gel-like consistency.

2.1.2 Assembly

3.33 mL of either ZeoLap or 3 mL of (HPLC-water), which have the same water content (Appendix A. 1), were pipetted to screw-capped 5 mL glass vials (VWR International, Längenfeld, Germany) with a small PTFE-coated magnetic stirrer. For each of the four atmospheric settings (Table 2.2.A), six types of samples were prepared: three for each medium (ZeoLap and water). Within each of the three, 1 mMol of metal atoms of Fe_3O_4 (231.53 mg) was added to one, and zero valence nickel nano-powder (177 mg) to another, leaving one without any metal added (Appendix A. 1 Mass characterization of each of the six different types of samples for ZeoLapLastly, the samples were mixed in a table vortex (1,500 rpm; Heidolph Instruments, Schwabach, Germany) until homogeneity was achieved and were subsequently covered with perforated PTFE screw caps to allow gas exchange inside the reactor[5,6]. For the next steps and assembly of the reactor, proceeded to “Reactor Setup”.

2.1.3 After Reaction Processing

The content inside each glass vial was carefully collected to a sterile 2 mL polypropylene syringe (B. Braun, Melsungen, Germany) connected to a polyethersulfone (PES) filter

membrane (pore size: 0.20 μm; SARSTEDT, Nümbrecht, Germany) and processed via hard filtration. The Zeolap mixture, together with the heterogeneous minerals, remained mostly on the filter. The remaining aqueous content was carefully extracted to 2 mL Eppendorf tubes. The liquid sample was then centrifuged (13,000 rpm; Biofuge fresco, Thermo Fisher Scientific, United States of America) for 15 min, transferred to new Eppendorf tubes, and centrifuged again to isolate any remaining particles in suspension.

Additional replicates were made to assure products were not lost in filtration, due to metal-carbon bonds formed during synthesis. Thus, in order to cleave such bonds through alkaline hydrolysis, replicates of water samples were made and processed differently, adding potassium hydroxide pellets (KOH pellets, Fisher chemicals, Loughborough, UK) to the glass vials immediately after reaction and mixing in a table vortex before transferring it to polypropylene syringes attached to a polyethersulfone (PES) membrane filter, as described above in this subsection[5].

2.1.4 Proton Nuclear Magnetic Resonance (^{1}H-NMR) Data Analysis

Products were identified using the standards described in Appendix B. 1. Any peaks detected besides DSS's and water's were considered contaminations or false positives in samples with Ar instead of CO_2 (Appendix A. 3 and Appendix A. 5). The baseline for runs done with CO_2 was thus set at the values obverted in each respective control[5,6].

2.2 Nicotinamide Adenine Dinucleotide (NAD) And Ionic Solutions

For all NAD related experiments a new protocol needed to be established, taking into consideration previous studies under similar hydrothermal conditions[6].

2.2.1 Sample Preparation

For all stock solutions, KOH pellets were added to HPLC-grade water with the assistance of a pH meter (alkaline water at pH 11; SCHOTT Instruments, Mainz, Germany), to be used as a solvent. A batch solution was made with 6 mM of NAD, twice the concentration needed for each sample. For that purpose, 39.8 g of NAD were placed in a beaker and diluted in 20 mL of the alkaline water. Then, it was gently mixed in a capped falcon tube until all visible particles dissolved, and a transparent homogeneous liquid was obtained.

Following the same protocol, the remaining solutions were made according to Table 2.1.

Table 2.1 Description of stock solutions for NAD experiments and their final concentrations

	Supplier	Mass (g)	Solution (mL)	Concentration (mM)
Sodium chloride (NaCl)	Carl Roth, Karlsruhe, Germany	11.70	10	20
Magnesium chloride Hexahydrate ($MgCl_2 \cdot {}_6H_2O$)	Carl Roth, Karlsruhe, Germany	40.70	10	20
Iron(II) chloride tetrahydrate ($Cl_2FeH_8O_4$)	Thermo Fisher Scientific, Schwerte, Germany	39.80	10	20
Iron (III) chloride anhydrous ($FeCl_3$)	Thermo Fisher Scientific, Schwerte, Germany	32.40	10	20
PIPES (≥99 % titration) ($C_8H_{18}N_2O_6S_2$)	Merck, Darmstadt, Germany	60.50	10	200

2.2.2 Assembly

For each set of experiments, four samples were prepared in 1 mL glass vials (VWR International, Langenfeld, Germany). Three of them were 1 mL replicates with one part of the 6 mM NAD batch solution and another equal part of a different solution (Table 1) or 77.10 mg of Fe_3O_4 in alkaline water. The fourth sample was a control containing alkaline water instead of the NAD solution. As an additional control, for every run, another four samples were prepared also using NAD's batch solution, but with a second part only containing alkaline water, as visually described in Figure 2.4. The same samples were prepared in 2 mL Eppendorf tubes and immediately measured as specified in "Spectrophotometric Analysis". The samples in the glass vials, however, were covered with perforated PTFE screw caps to allow gas exchange and placed on a stainless-steel reactor. For more details on the preparation of these samples, placed in the reactor, proceed to "Reactor Setup".

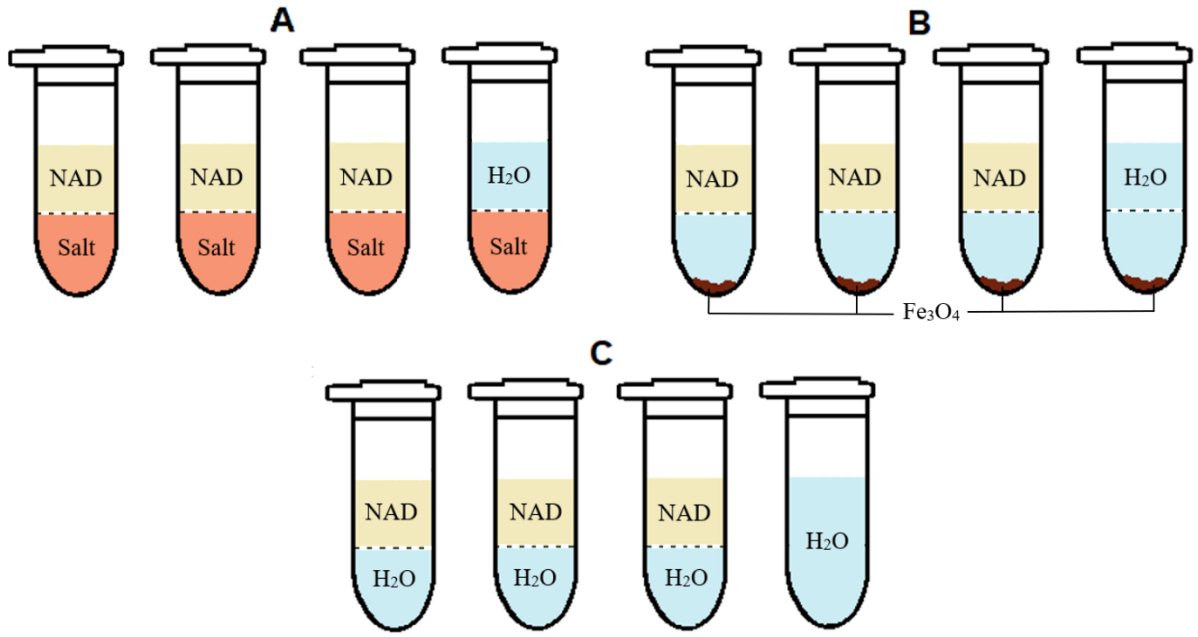

Figure 2.4 Figurative representation of the different parts that were mixed to obtain the pretended solution. In laboratory conditions, the different liquid phases mixed into a homogeneous solution, but the magnetite (Fe_3O_4) persisted mostly as a precipitate; A: Example of the parts of a sample with a salt solution (red) and a solution of NAD (yellow). Samples with PIPES and NAD would be prepared similarly; B: Example of the parts of a sample with magnetite (Fe_3O_4) and NAD. To dilute the NAD solution to half of its concentration, an equal part of water was added. Samples that also contained a part of magnesium chloride in solution would not require the addition of water; C: Figurative representation of the different parts of NAD controls.

2.2.3 After Reaction Processing

Samples that did not contain any form of iron were immediately measured in the spectrophotometer, as described below ("Spectrophotometric Analysis"). As per samples containing iron (as salt or mineral), 10 µL of 0.5 mM KOH were added to each sample to facilitate precipitation. The solutions in the glass vials were transferred to 2 mL Eppendorf tubes and centrifuged at 13,000 rpm for 15 min. Afterward, the supernatants were transferred to new Eppendorf tubes and centrifuged again, leaving behind a pellet with any amount of precipitated iron. The remaining supernatantwas then analyzed in the spectrophotometer.

2.3 Reactor Setup

All tubes were placed vertically in a stainless-steel reactor (Berghof Products + Instruments, Eningen unter Achalm, Germany), and the reactor lid carefully locked to create a controlled system that could be either an open system, allowing gas exchange through the lid valves or a closed system during the reaction, allowing heat exchange through the reactor walls. Before introducing the reaction gases to the reactor, it was flushed with 5 bar of Ar gas three times to

replace the internal atmosphere. Afterward, gases were added as presented in Table 2.2 and brought to a final pressure of 25 bar for the Zeolap experiments and 10 bar for the NAD experiments. Finally, the reactor was placed in a heating mantle (Heidolph Instruments, Schwabach, Germany) with the experimental required settings for stirring, temperature, and time (Table 2.2). The system inside the reactor heated slowly from room temperature until the tabled value and maintained it for the duration of the experiment, starting to cool down once the timer reached zero. As soon as the reactors cooled to approximately 35 °C, they were depressurized, removed from the heating mantle, and opened to recover the samples[5,57].

Table 2.2 A) Setup of the reactor after closing it for ZeoLap experiments. Two different setups were tested composed by CO_2+H_2 and CO_2+Ar and two other setups for the respective controls H_2+Ar and Ar. Each gas was introduced to the system in the indicated order until a final pressure of 25 bar was reached. The purity of these gases was 99.999 %, 99.998 %, and 99.995 % for H_2, Ar, and CO_2, respectively; B) Reactor setup after closing for NAD experiments. Two different setups were tested, composed of 2 bar of H_2 and 10 bar of the same gas, and two other setups for the respective controls with Ar. The purity of these gases was 99.999 % and 99.998 % for H_2 and Ar, respectively.

A	CO_2 + H_2	CO_2+ Ar	H_2 + Ar	Ar
1st	10 bar of H_2	10 bar of Ar	10 bar of H_2	25 bar of Ar
2nd	15 bar of CO_2	15 bar of CO_2	15 bar of Ar	-
Specifications	1,400 rpm; 70 ºC; 16 h			

B	H_2		Ar	
Pressure	10 bar	2 bar	10 bar	2 bar
Specifications	30 ºC; 2 h			

2.4 ^{1}H-NMR Analysis

Immediately after sample processing, 600 µL of supernatant was collected from the centrifuged samples to a fresh batch of Eppendorf tubes containing 100 µL of a solution comprising 0.7 mM of DSS in deuterium oxide (D_2O), and the same protocol was applied once more for centrifuging. The ending result was transferred to NMR tubes and capped (VWR International, Längenfeld, Germany). Lastly, these probes were analyzed on a Bruker Avance III – 600 MHz at 297 K, using a ZGESGP pulse program. Each sample was scanned 32 times with a relaxation delay of 40 s, and a spectral width of 12,315 ppm. Spectra analysis and integration were performed using MestReNova (10.0.1 version) software[5].

2.5 Ultra-High-Performance Liquid Chromatography (UHPLC) Analysis

After concluding "After Reaction Processing", 400 µL of supernatant was pipetted to fresh 1 mL glass vials (VWR International, Längenfeld, Germany). A Dionex UltiMate 3,000 Standard Systems UHPLC machine (ThermoFisher, United States of America) with a LC column - Rezex ROA-Organic Acid H+ (8 %; Phenomenex, Aschaffenburg, Germany) - was used for sample analysis through flexible UV-Vis absorbance detection. Spectra analysis and data collection were completed using Chromeleon (7 version) software[6].

2.6 Stereomicroscopy

Dried samples of ZeoLap were observed in a Nikon SMZ18 Stereo Microscope (Nikon, Japan), the respective digital images collected by a DS-Ri1 Digital Microscope Camera (Nikon, Japan) and obtained from NIS-Elements SMZ18 software.

2.8 Spectrophotometric Analysis

1 mL of each NAD sample was pipetted into 1mL plastic cuvettes for analysis on the visible (tungsten lamp) and ultra-violet spectrums (UV; deuterium-halogen lamp) with a DU 800 Spectrophotometer (Beckman Coulter, Sinsheim, Germany). Through the DU 800 UV/Vis Spectrophotometer software, samples were analyzed at fixed wavelengths (260 nm, 280 nm, and 340 nm), and it was obtained wavelength curves of the totality of both visible and UV spectrums.

2.9 Water activity (a_w)

Preliminary tests were done to evaluate water activity of ZeoLap samples. Pure water is usually used as a reference in a_w tests, corresponding to the maximum value of one. To assess the impact that clays could have on this front, HPLC-grade water was used as a standard in the tests performed using a_w measuring instrument (LabMaster-aw neo, Novasina AG, Lachen, Switzerland) with a CM-3/awSens-ELS sensor and samples with different concentrations of Zeolite, Laponite and salts were tested (Table 3.4).

3. Results and Discussion

3.1 Laponite-RD and Zeolite experiments

3.1.1 Protocol development

During this work, two different media were tested. The results helped to compare the role of different frameworks and media in CO_2 reduction: water and ZeoLap. Water samples that were dealt with in the exact same way as ZeoLap samples will be called “WaterS”. Water samples, to which was added a KOH pellet after the reaction, will be called “KOHS”. Thus, ZeoLap samples will be called “ZeoLapS”.

While developing the protocol for a Laponite-RD and Zeolite based clay, numerous data was collected over a broad set of variants that could help to build the best framework. This clay should provide a porous framework for the experiments while still being manageable in the laboratory, both for assembly and analytic purposes, and also be appropriate in the hydrothermal vents’ context. Limitations encountered during this process were:

- The structure of the clay was sensitive to variations in the water pH, leading to a heterogeneous solution with separated liquid and solid phases when the sample’s pH was too acidic.
- Water loss by evaporation either before or during the reaction would make the clay too rigid, making it unfeasible to filtrate. It was important that each beaker was covered during the preparation of samples and did not use temperatures of 100 ºC or higher during reactor runs, limiting them to 70 ºC.
- The first type of Laponite used was Laponite-EP (BYK chemicals, Wesel, Germany), which proved to contain remaining organic matter, overflowing results with a significant amount of contamination (Appendix A. 2)
- A homogeneous gel was hard to obtain with Laponite-RD concentrations lower than 3 % (Figure 3.5.B), and higher concentrations than 7 % made it too rigid. Because this material still showed some contamination (Appendix A. 5), it was used the lowest percentage possible (2.7 %), requiring an additional mixing time of 1h to obtain homogeneity.

The protocol used to prepare samples before analysis and during analysis was based on Preiner's et al. work on samples with hydrothermal vents' minerals and conditions in water[6] and adapted to correspond to the restrictions of having a gel-like framework.

3.1.2 Sample characterization

To provide a more fair-minded comparison between both media used in this work, they were characterized by pH, water activity (a_w), and structure (Table 3.3, Table 3.4, and Figure 3.5, respectively). The water pH was adjusted to match ZeoLap's initial conditions before the reaction occurred. Continuously, every sample contained the same amount of water (3 mL), and a more detailed characterization of their composition can be found attached (Appendix A. 1)

Table 3.3 Description of punctual alterations of pH of a standard ZeoLap sample and a standard water sample.

	ZeoLap	water
Initial	10.6	10.5
After 1h Mixing	10.5	
After reaction	8.0	4.8

Even though both media would have the same starting point, ZeoLap would maintain an alkaline pH during the reaction, acting as a buffer. Water media showed to have a significant decrease, observable after the reaction (Table 3.3), a consequence of CO_2 uptake by water and subsequent synthesis of carbonic acid[58]. While adding KOH to water samples after the reaction assumedly reestablished an alkaline environment, the 16 h long reaction of KOHS still ran under the same conditions as waterS. Whereas having a controlled alkaline environment favors reduction, the oxidizing properties of acidic media such as water samples might inhibit the reduction of CO_2.

Table 3.4 Water activity essay on different media. These media include ZeoLap with different concentrations of Laponite and Zeolite, highly saturated salt solutions, and ZeoLap (2.7 % of Laponite) prepared in these same salt solutions instead of ultra-pure water.

Medium tested	Water activity (a_w)	Bond water (%)
Control (ultra-pure water)	1.000	0.0
7.3 (%w/w) of Laponite and 2.7 (%w/w) of Zeolite in ZeoLap	1.010	-1.0
4 (%w/w) of Laponite and 6 (%w/w) of Zeolite in ZeoLap	0.998	0.2
6 (%w/w) of Laponite and 4 (%w/w) of Zeolite in ZeoLap	0.997	0.3

2.7 (%w/w) of Laponite and 7.3 (%w/w) of Zeolite in ZeoLap	0.989	1.1
Supersaturated $CaCl_2$ Solution	0.241	75.9
5 M $CaCl_2$ Solution	0.581	41.9
ZeoLap mixture in 5 Molar $CaCl_2$ Solution	0.571	42.9
Supersaturated $MgCl_2$ Solution	0.398	60.2
$MgCl_2$ Solution (Unknown Concentration)	0.791	20.9
ZeoLap mixture in $MgCl_2$ Solution (Unknown Concentration)	0.777	41.9

Preliminary water activity tests were made to determine the amount of free water in ZeoLapS. Conventionally, pure water corresponds to a maximum reference value of one, where 100 % of the water is free, and 0 % is bond water. Thus, waterS and KOHS, which media was ultra-pure water, have $a_w = 1$. Results revealed that the percentage of Zeolite in the clay is inversely proportional to water activity measurements in ZeoLapS. This aligns with previous studies which suggest that most zeolites absorb less than half of its mass in water[59]. Accordingly, with an overall weight by weight percentage of clay materials of 10 %, a_w reduction was predictably less than 5 %. With the addition of Laponite, ZeoLap presents a much wider porosity than typical zeolites, which also leads to a decrease in the amount of bond water[60]. Although silica gels and zeolites are materials commonly used for their high sorption capacity, hygroscopic salts are known to be significantly better. Hence, highly concentrated saline solutions presented a much more significant a_w reduction, being its lowest when supersaturated. Mixing ZeoLap in magnesium chloride and calcium chloride solutions showed to have an additive result but lead to the precipitation of the clay. This behavior has already been observed in other salt-silica gel composites that have better water sorption than either of the materials individually[61,62]. However, the de-gelling of ZeoLapS constitutes an irrevocable disadvantage for the purpose of this work.

Structurally, ZeoLapS presented the open and irregular porous structure that was pretended (Figure 3.5.A) to simulate the internal structure of hydrothermal vents, with pore size up to 1 mm. Nickel and magnetite integrated quickly in the structure, being accessible to the reactants on the surface of the pores.

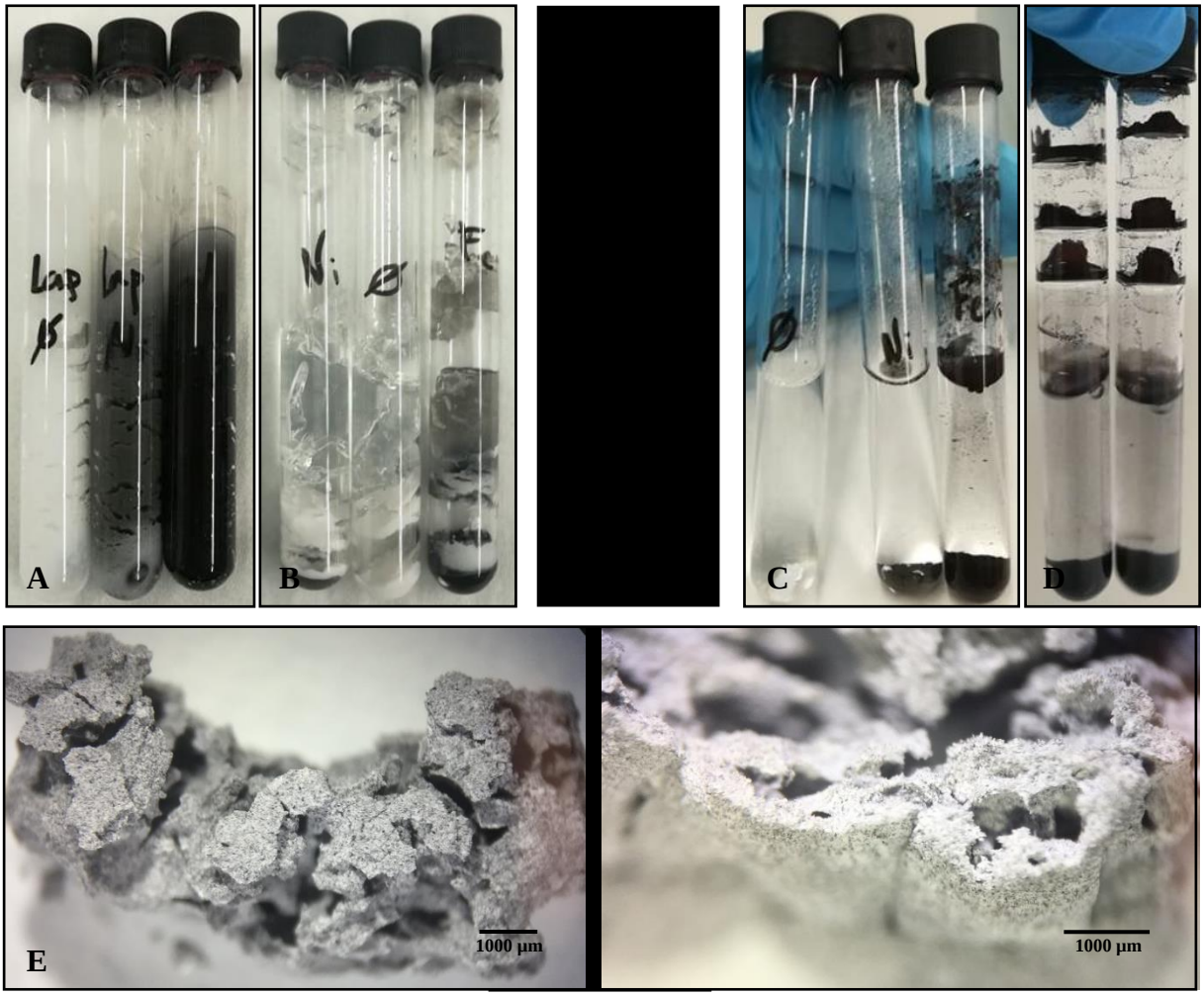

Figure 3.5 ZeoLap and water samples after reaction and after slow drying. A) The gel-like ZeoLap mixture placed into the reactor would lose some water, during the 16 h experiment at 70 ºC, and obtain a firmer porous structure. From right to left there are tubes with only the ZeoLap mix, ZeoLap with nickel powder and ZeoLap with magnetite; B) During the development of the protocol, samples with low concentration of Laponite or a short mixing time would present a similar result, where both the ZeoLap powders and the added metals did not mix properly and would deposit at the bottom of the tube; C) Structureless water samples collected from the reactor, after a 16 h experiment at 70 ºC. From right to left there are tubes with samples with only water, water and nickel powder and water with magnetite; D) Water samples with magnetite would often form a solid disc of oxidized iron, dividing the gas phase; E) The structure of ZeoLapS is visible through stereomicroscopy. To preserve its structure, it was dried slowly at 70 ºC for 5 h in an oven. The added metals would evenly distribute over the surface of the gel, in a granular pattern.

Water samples, as mentioned before, did not provide any framework for the reactions to occur, but the stirring would help to increase the contact surface area between the metals and water. Samples containing magnetite presented solid discs after the reaction, above the solution, as in Figure 3.5.D. This barrier could limit iron oxidation and, consequently, the synthesis of other reduced forms of carbon[6].

3.1.3 Final data

Complementary to the work developed by Preiner et al., samples were screened for acetate, ethanol, formate, methanol, and pyruvate detection and quantification. All products were not only detected in standard samples but also controls (CO_2-free). Most importantly, methanol and ethanol were detected consistently in every control, before and after the reaction, meaning that contamination was still a considerable problem **(**Appendix A. 3 and Appendix A. 5**).** Despite all materials used being assumedly sterile and not containing organic compounds, working on a micromolar scale proved to be an inherent limitation, detecting even the smallest of contaminations.

After considering all contaminations, the concentrations of methanol and ethanol in most samples were revealed to be either insignificant or arbitrary. The lack of an observable pattern indicates that they are most likely only contamination and not synthesized during the reaction. However, because the background contamination is so high, we cannot entirely exclude the possibility that these molecules are being synthesized in small quantities.

Formate, as expected, was found in higher concentrations in nickel-containing samples[63–65]. Its synthesis was more pronounced in water samples, up to 106.8 µM in waterS and 152.5 µM in KOHS (Figure 3.7). It is the first intermediate product of the acetyl-CoA pathway, leading to the synthesis of acetate (Figure 1.1)[66,67]. Thus, composing the initial stage of CO_2 reduction, formate is essential for the synthesis of more complex molecules but also a product of their degradation. Even though all experiments started under alkaline conditions, water samples presented a final pH as low as 4.8, which could promote the oxidation of other hydrocarbons synthesized at the beginning of the reaction, to produce formate, in addition to CO_2 reduction (equation (3.1)). Overall, it was the product found in higher concentrations, as similar studies have reported from H_2 and CO_2[68,69], and from CO_2 with hydrothermal minerals and native metals[5,6,70]

$$H_2 + CO_2 \rightarrow HCOO^- + H^+ \quad (3.1)$$

Contrastingly, acetate was not found in waterS above the contamination threshold, and concentrations of this molecule were found in KOHS up to 5.09 µM (Figure 3.7). Acetate has an additional methyl group than formic acid and occurs five steps later in the acetyl-CoA pathway than formate[3,66] (). Primarily, it could be speculated that by increasing the sample's pH after the reaction, reducing conditions would favor the synthesis of more complex hydrocarbon species such as acetate (equation (3.2)). However, this reaction is endergonic at

room temperature, requiring either high CO_2 concentrations or a good catalyst[71]. In addition, it would lead to the consumption of formate, which, even in the presence of catalysts and at 100 ºC, catalysis is not far on the side of acetate synthesis (equation (3.3))[6]. Lastly, the production of acetate in KOHS does not seem to be associated with a reduced amount of formate in the same samples, compared to waterS. On the other hand, it is likely that both KOHS and waterS are producing similar amounts of acetate, as the conditions during the reaction are identical, and the difference observed is due to alkaline hydrolysis that breaks metal-carbon bonds and frees acetate to be quantified.

$$4H^2 + 2CO_2 \rightarrow CH_3COO^- + 2H_2O + H^+ \quad (3.2)$$

$$3H^2 + CO_2 + CHOO^- \rightarrow CH_3COO^- + 2H_2O \quad (3.3)$$

Analysis of ZeoLapS revealed the highest production of acetate out of all samples. Given the constant alkaline conditions and the low concentration of formate detected, it is possible that, contrary to what was discussed previously, the reduction of CO_2 to acetate was vastly favored over the accumulation of formate on these samples.

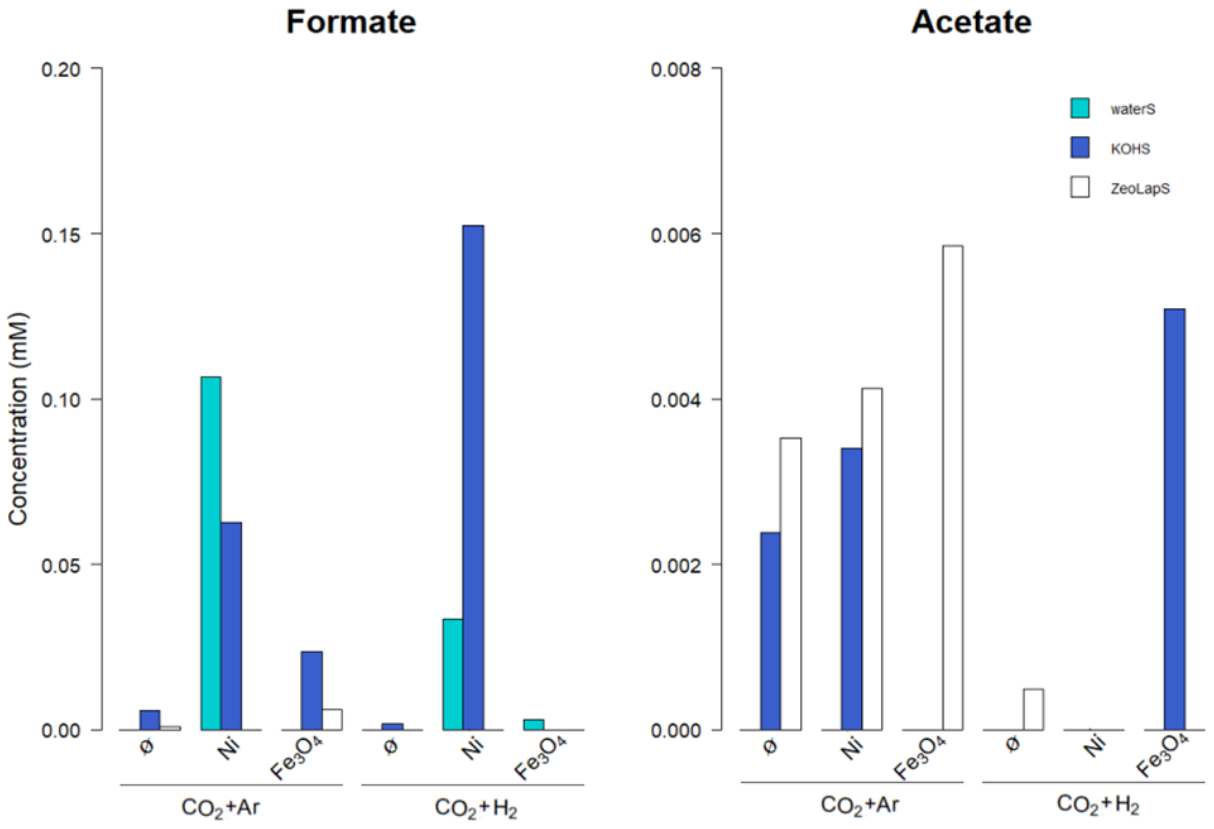

Figure 3.7 Formate and acetate as a product of CO_2 reduction compared between waterS, KOHS, and ZeoLapS. All samples had 15 bar of CO_2 in addition to 10 bar of Ar or H_2, to a total of 25 bar. In addition, samples could have magnetite (Fe_3O_4), nickel (Ni)

Previous experiments revealed that iron plays an indispensable role in catalyzing the synthesis of pyruvate, and again it was only observed in magnetite containing samples[5,6,72]. Approximately 24 µM of pyruvate were produced in waterS (magnetite, CO_2 + Ar), but it was not observed pyruvate to the same extent in any other medium nor conditions, possibly being contamination. In ZeoLapS (magnetite, CO_2 + Ar), a two-fold smaller amount of pyruvate was detected, matching similar quantities to what previous studies reported[5,6]. However, these same studies also reported pyruvate to be produced in water, which was not reproduced in this work. The lack of pyruvate can be explained due to various reasons. This molecule is found in low concentrations, even compared to other products. Thus, contamination quickly rejects any amount of pyruvate detected. Additionally, magnetite could be oxidized before the reaction, not playing its role in the reaction. Finally, these results are based on small sample sizes, possibly misrepresenting the truth.

Overall, runs performed without H_2 lead to more product accumulation, despite CO_2 reduction being more favorable with H_2. Controls were contaminated with organic molecules previously to reactor runs, as it was already mentioned. Possibly, these compounds also reacted and produced molecules in similar patterns to our samples, increasing the threshold for contamination. Accordingly, controls with H_2 had higher background contamination than controls with only argon, as shown in attachments **(**Appendix A. 3 and Appendix A. 5).

3.2 Nicotinamide adenine dinucleotide (NAD) reduction experiments

3.2.1 Controls

The stability of NADH was tested in ultra-pure water and a 0.1 M PIPES solution throughout 2 h and 24 h at room temperature (Figure 3.8). A minimal decrease in concentration was observed over time, independently of the medium. In any case, less than 5 % was lost over 24 h, proving to be extremely stable. This suggests that if a certain amount of NADH was to be synthesized during the experiments, it would mostly remain stable in solution.

For the purpose of this work, absorbance values were corrected by subtracting the average absorbance detected in each triplicate control (ΔA, NAD-free). The NAD^+ spectrum, which peaks at 260 nm, extends its curve over 340 nm (NADH peak's wavelength) in the concentrations used (Figure 3.1213). Because absorbance is additive[73] the difference of ΔA measured before and ΔA measured after the run was calculated (ΔΔA) to detect NAD^+

reduction, and NADH synthesis was considered only when ΔΔA was positive. ΔΔA was also calculated for additional controls, with Ar instead of H_2, and both values were compared to discuss if hydrothermal conditions can reduce NAD^+.

Table 3.5 Reference table for NAD's data processing and calculus.

	Ar	H_2
Raw data: absorbance at 340 nm	A	A
Correction values: ΔA	$A_{NAD} - A_{Control}$	$A_{NAD} - A_{Control}$
Progression during reaction: ΔΔA	$\Delta A_{after} - \Delta A_{before}$	$\Delta A_{after} - \Delta A_{before}$
Final value	$\Delta\Delta A_{Ar}$	$\Delta\Delta A_{H2}$

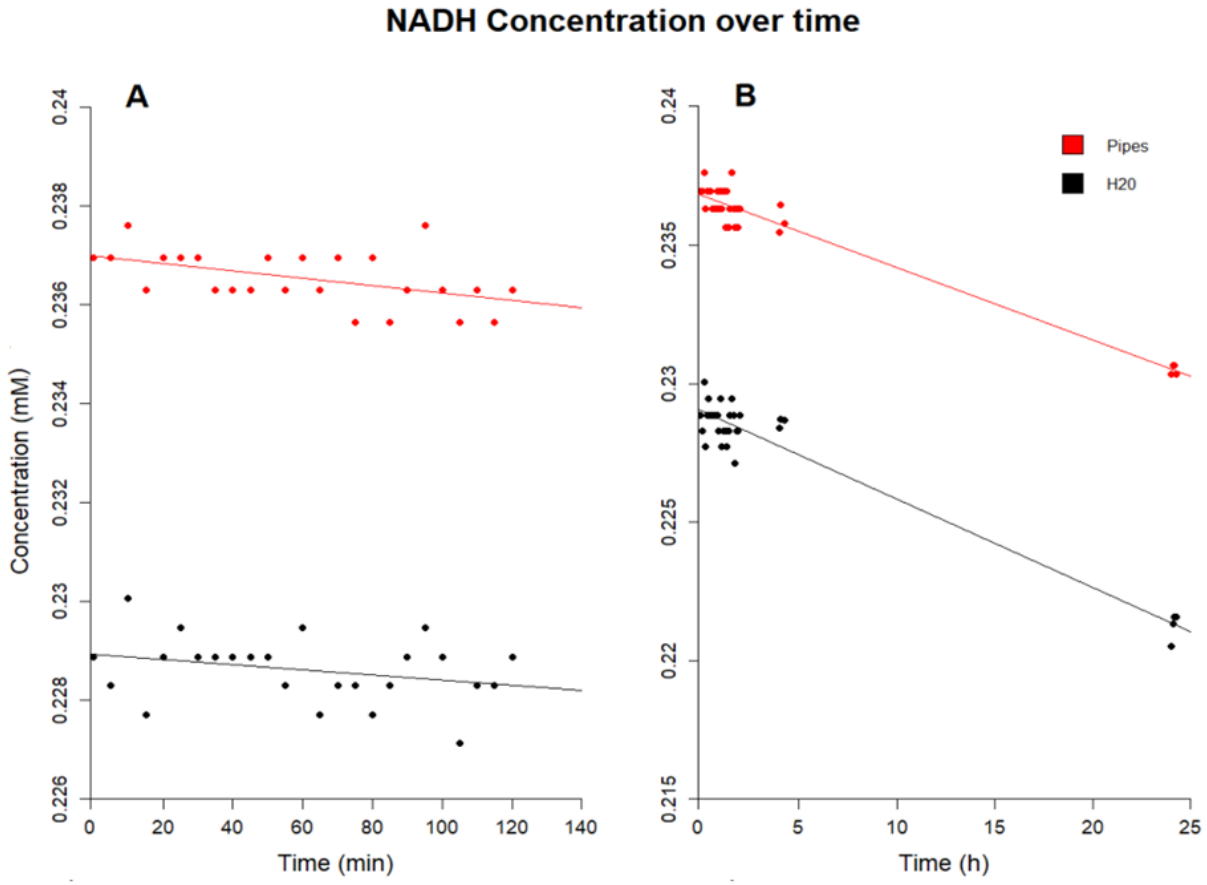

Figure 3.8 The determined degradation rate of NADH is 4 $nm.min^{-1}$ over 24 h (graph B, y = – 4E – 6x + 0.2368, R^2 = 0.945) in a PIPES solution and 5 $nm.ml^{-1}.min^{-1}$ in ultra-pure water (graph A, y = – 5E – 6x + 0.229, R^2 = 0.936).

Unpredictably, most controls with Ar revealed to have a positive ΔΔA. Even though H_2 can be generated from water by native iron and other reductants, an increase in ΔA was also observed

in samples with only water and NAD^+. The opposite behavior was expected, as NAD^+ should start degrading, and the overlap at 340 nm diminish. This could be attributed to errors in the preparation of the replicates. The variance introduced by human hands is likely more noticeable than the prolonged degradation of NADH. On the other hand, this can suggest that in the absence of H_2, other reactions are occurring and affecting absorbance measurements.

Even though using different iron sources is useful for the purposes of this work, it constituted some difficulties. Dissolved iron has color and can affect spectrophotometry measurements. Thus, before analysis, KOH was added to each sample containing iron to precipitate and break any metal-carbon bonds. To study the effects that KOH can have in NADH's stability, it was measured the absorbance of different NADH solutions with known concentration with or without KOH (Figure 3.89). At the concentrations used, no significant difference was observed between controls. This indicated that if any NADH is present after the reaction, the additional variant and the drastic change in pH (

Appendix C. 1), should not affect the spectrophotometric analysis.

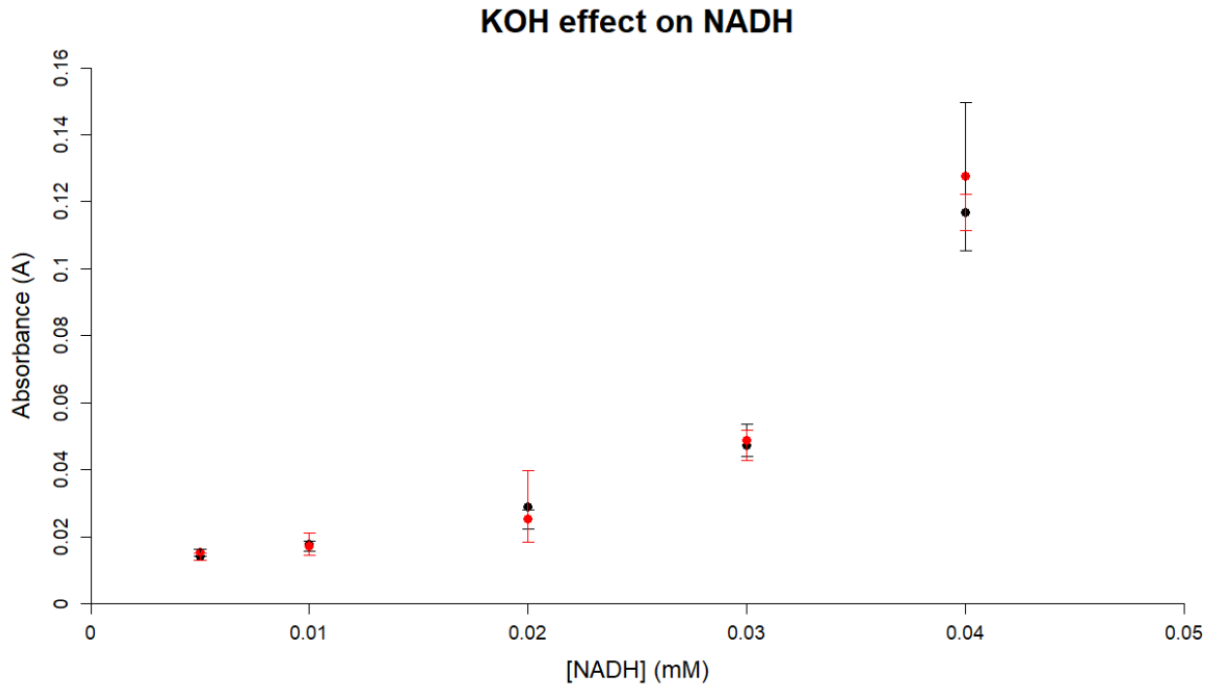

Figure 3.8 Average absorbance of 5 different concentration of NADH in between 0,005 and 0,05 mM with (red) and without (black) adding KOH to the solution.

To further investigate the possible consequences of using KOH, absorbance was measured at 340 nm for two hours after adding KOH to a solution of 3 mM NAD (Figure 3.910).Over a period of ninety minutes, the absorbance measured almost doubled, stabilizing afterward. In the

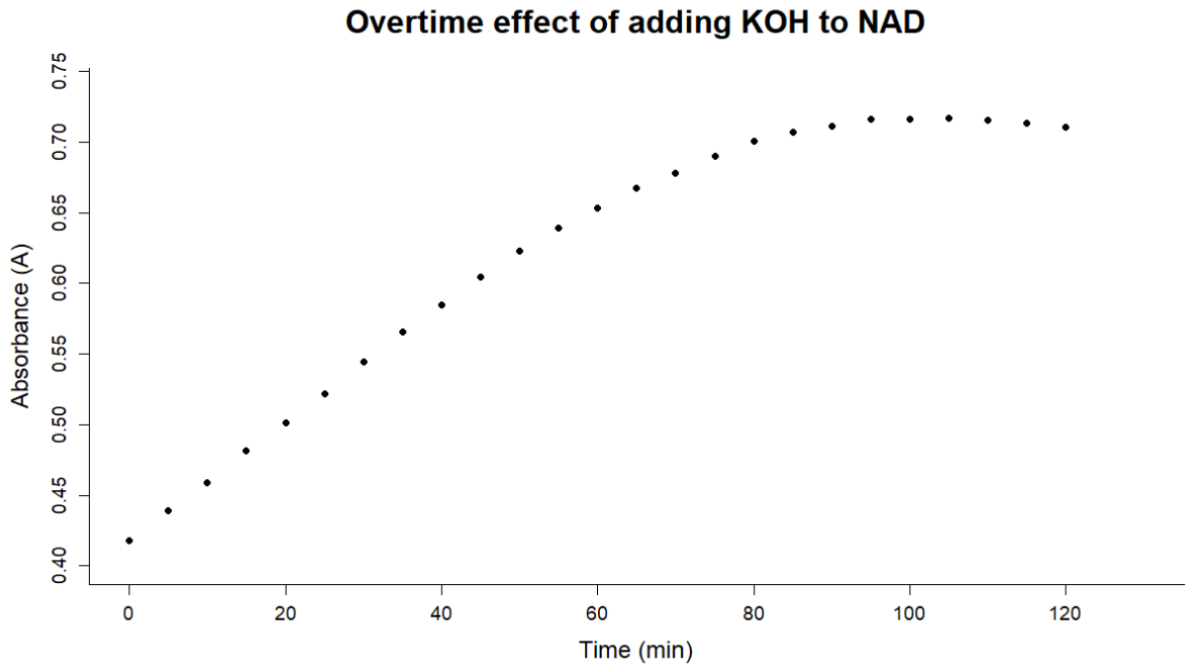

Figure 3.9 Absorbance (340nm) progression every five minutes after adding 10 µL of 0.5 M of KOH to 3 mM of NAD at time zero.

absence of a catalyst or even a hydrogen source, an increase of absorbance over time indicates once more that secondary reactions are most likely happening and affecting measurements. Although KOH is only added after the reaction run is completed, measurements are made after two fifteen minutes long centrifugations, enough time for absorbance to potentially increase 140 % at 340 nm. These controls can partially explain why Ar controls have high absorbance values, but KOH was only added to iron-containing controls and samples, leaving the rest of the observed values to unknown sources. Assuming the same secondary reactions are occurring in controls and samples, except for NAD reduction, then a difference in absorbance should be detectable.

3.2.2 Final data

The transition from the oxidized state to the reduced state of NAD in water requires the transfer of a hydride (equation (3.4)). In the laboratory setup, hydrogen was added to the system as a gas, which does not dissolve in water easily[74]. Thus, to improve solubility, samples were tested at different pressures and compared.

$$NAD^+ + H_2 + H_20 \rightarrow NADH + H_3O^+ \quad (3.4)$$

At only 2 bar, none of the samples showed consistent results. After two hours in the reactor, only samples with NAD^+ and with both NAD^+ and NaCl had a significant increase in

absorption. Generally, samples that displayed an increase in absorbance relative to their controls ($\Delta\Delta A_{Ar} < \Delta\Delta A_{H2}$) were considered positive results, as if there was NADH synthesis. However, as mentioned before, only positive $\Delta\Delta A_{H2}$ can be considered, even if $\Delta\Delta A_{Ar} < \Delta\Delta A_{H2}$ is still observed. Thus, data that only obliged to the first rule and not to the second was highlighted in red as a false positive in 10. Overall results seem arbitrary. The difference between $\Delta\Delta A$ was biggest with only ultra-pure water and NAD^+ (0.03314 $\Delta\Delta\Delta A$; 14.47 µM NADH), and there was no reductant involved in the reaction. Thus, it would be expected that other samples with reductants would present better results.

The addition of salts and minerals to the solutions did not show a positive effect on NAD^+ reduction. Except for NaCl, all of these samples presented either a lower absorbance than its respective control with Ar or a decrease in absorbance during the reaction. What was observed was that these compounds lead to a substantial decrease in the solution's pH (Appendix C. 1), which can easily cause NAD^+'s degradation[53,56], hence the values observed.

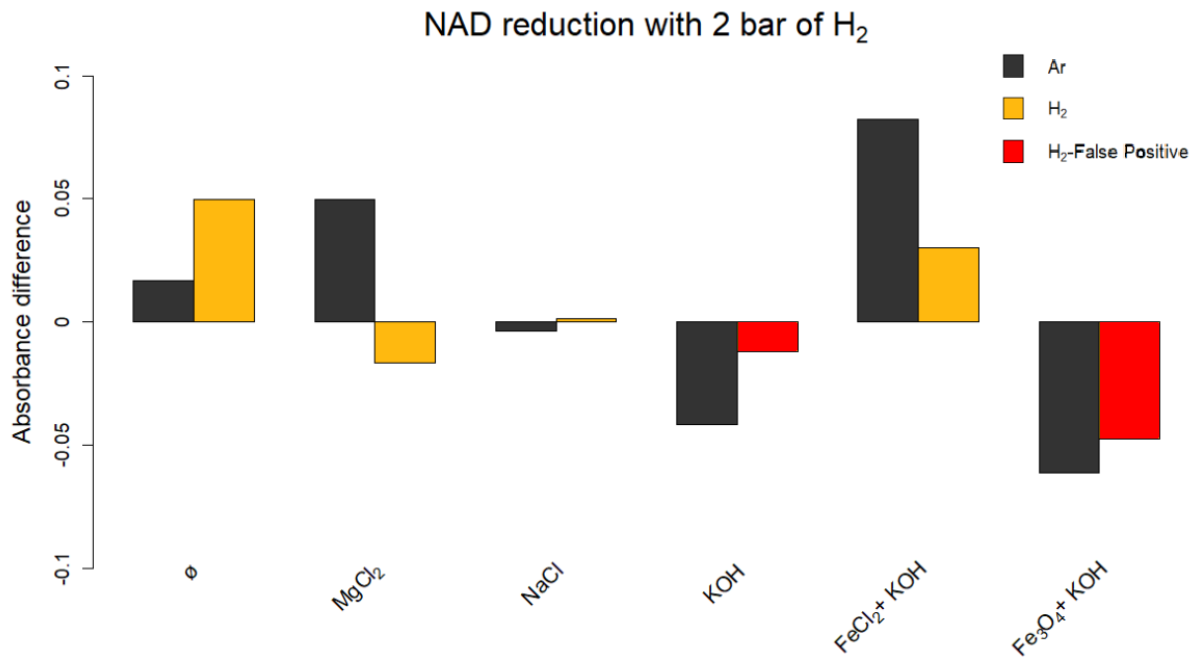

Figure 3.10 Compared side by side are controls made with 2 bar of argon (black) and results obtained with 2 bar of H_2 (yellow and red). Samples which values are higher than the respective control but still negative are highlighted in red, as false positives. Each bar represents the progress of absorbance values from before the reaction to after the reaction ($\Delta\Delta A$), in argon or molecular hydrogen.

At 10 bar, however, results were more consistent, and the discrepancy between controls and samples was sharper (Figure 3.1112). Samples with iron performed the best out of all tested, increasing its absorbance the most, noticeably a mixture of magnetite and magnesium chloride

(0.339 ΔΔΔA; 147.91 µm/mL NADH). All samples without iron did not increase in absorbance compared to their controls, and the variation between ΔΔA was smaller.

Even so, results are not precise. An accentuated increase in absorbance does not imply that a more significant concentration of NADH is in the sample compared to a different sample were an increase was also observed. Most samples have more than one variable that differentiates them from another. Consequently, it is essential that we only compare them to their own control. For example, besides the salt in solution or the mineral added, parameters such as solution pH, which was dependent on the salt solution used, and KOH treatment, vary across samples, making it harder to compare results.

Possibly, samples that were considered false positives can be a result of both NAD^+ degradation ($\Delta\Delta A < 0$) and NAD^+ reduction ($\Delta\Delta A_{Ar} < \Delta\Delta A_{H2}$), but given the unpredictability of results observed at 2 bar, such a conclusion would require a more in-depth analysis.

Magnesium salt alone did not catalyze NAD reduction, but potentially facilitated magnetite's catalysis, leading to a significant increase from $\Delta\Delta A_{Ar}$ to $\Delta\Delta A_{H2}$ when compared to samples with only magnetite or $MgCl_2$. Magnesium is a material of growing interest in the industry for hydride transfer[75–77]. It has excellent hydrogen storage potential, reacting to form magnesium hydride (MgH_2), but the reverse reaction is highly endergonic. In the absence of a catalyst or high temperatures (> 250 ºC), the magnesium hydride retains the hydrogen, which aligns with the results found in samples only with magnisium[78]. For hydride transfer porposes, many metal composites, some with iron and magnesium, have been developed to facilitate the hydride desorption without affecting its absorpion[78,79]. Even though our experiments do not use such materials, magnetite could have an impactful role in the transfer of the hydrogen, as we have seen its effectiveness before for CO_2 reduction.

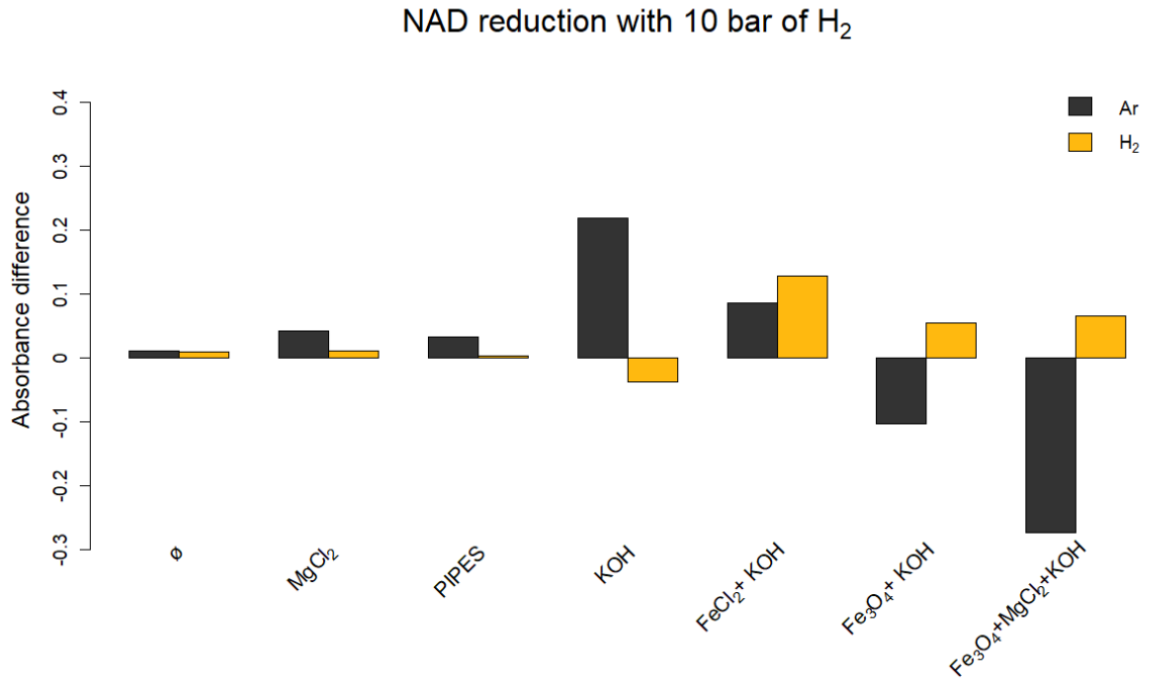

Figure 3.11 Compared side by side are controls made with 10 bar of argon (black) and results obtained with 10 bar of H_2 (yellow). Each bar represents the progress of absorbance from before the reaction to after the reaction (ΔΔA), in argon or molecular hydrogen.

Since NAD^+ has a different spectrum from NADH, NAD^+'s reduction in the presence of magnetite should be confirmed by obtaining the spectrum of this solution after reaction. Thus, a schematic representation of the spectrums (Appendix B.1) of NAD^+ and NADH before and after the reaction is in 12. Reinforcing the discussion of **Erro! A origem da referência não foi encontrada.**8, where it was stated that KOH does not affect the spectrophotometric analysis of the reduced form of NAD, the spectrum defined by NADH in the presence and absence of KOH are visually identical. NAD^+ alternatively has two different spectrums, in red and blue, also supporting the ideas already discussed. Noteworthy is the difference between adding KOH to NAD^+ in solution and adding KOH, after the reaction (30 ºC, 10 bar H_2), to a solution with NAD and magnetite. The first has a large peak that extends itself past 340 nm and has similar to the absorbance of a 0.05 mM NADH solution, at 340 nm. The second, after the reaction, has 2 distinct peaks. The added peak observed at 340nm matches the peak of NADH's spectrum, which suggests that the reduction of NAD^+ is in fact happening. Lastly, it seems that there are two different mechanism that lead to an increase of absorbance at 340nm but while it is not clear which reactions occur as consequence of mixing KOH and NAD, it seems highly likely that magnetite can catalyze NAD^+ reduction with H_2 as a simple abiotic source of hydrides.

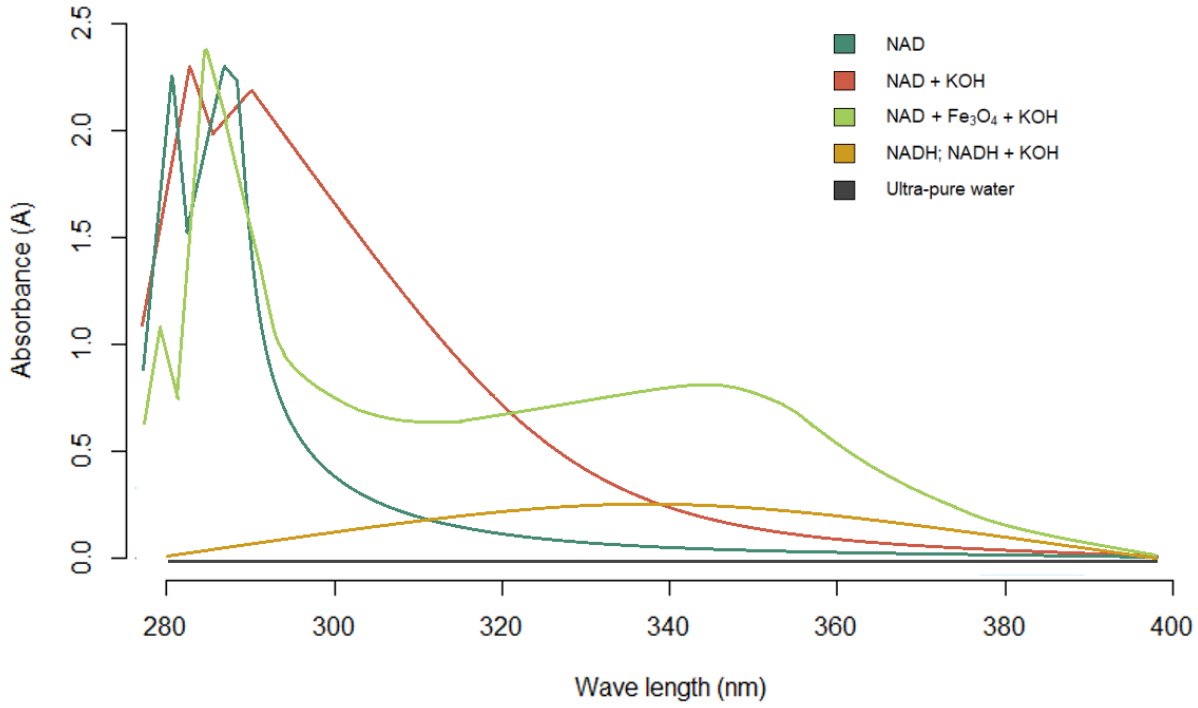

Figure 3.12 Schematic representation of spectrophotometric curves based on Appendix B. 2. Samples were prepared individually and measured. All samples with NAD^+ had 3 mM of this molecule, and samples with NADH had only 0.05 mM. In blue its represented the final segment of NAD^+'s peak at 260nm, which extends when KOH is added (red). With magnetite (Fe_3O_4), after a 2 h long reaction (30 ºC, 10bar H_2), adding KOH does not provoke the same effect, appearing a different peak at 340 nm (green). In yellow are represented both curves for NADH and NADH with KOH, as they overlap, and in gray a control with only water.

4. Conclusion

An open mesoporous framework was effectively developed to represent the structure of alkaline hydrothermal vents. For analytic proposes, however, it constituted a significant barrier, as there was a significant amount of contamination. In addition to the clay being contaminated, it was also persistently in the laboratory materials used. Contrastingly, the filter proved to cause product retention. In future experiments it is essential to increase sample size, but more meaningful results would be obtained simply by using pure materials and sterile single-use utensils, in addition to previously testing them for product retention. Even so, ZeoLap tended to promote the synthesis of longer molecules (acetate and pyruvate), while water samples produced mostly formate. This predisposition is shared among many porous materials and is what makes layered silicates of most interest in catalysis[17,42]. During this work, the production of specific molecules was observed. For future studies, it could be of most interest to examine if a porous framework could promote the reduction of CO_2 even further within the metabolic pathway. To move in this direction, controlling hydrolysis would be an essential step to take. Alkaline hydrothermal vents' water is rich in oxidized minerals and salts, which bind to water and reduce its activity. While water can act as a catalyst for both reduction and hydrolysis, in aqueous solutions, hydrolysis reactions are often favored over synthesis. Conventionally, pure water corresponds to a maximum reference value of one. Thus, high water activity values are associated with increasing hydrolysis. Synthesis is accordingly favored more often when a_w values are closer to zero[80]. In this study, mixing ZeoLap with supersaturated solutions leads to its precipitation, as the clays need free water to form its layered structure. Thus, assessing what concentration of salt ZeoLap can tolerate without precipitating could lead to exciting reduction experiments in the future. Overall, results suggest that the porous structure of hydrothermal vents could have had a significant impact on the origin of metabolism, the acetyl-CoA pathway, and organic matter, by shifting the thermodynamic equilibrium in favor of longer hydrocarbons.

The stability and reduction of NAD^+ were also studied. Once again, the most significant limitation was in methods and materials. Spectrophotometric analysis is sensitive to any emission in the same wavelength, independently of its source, which leads to a significant amount of variability in our results, especially at 2 bar. Other techniques, such as ^{13}C-NMR or ^{1}H-NMR, can distinguish NAD^+ from NADH better, such as other side products that might be affecting our results. A better collection of information about what is in solution could lead to more complete understanding of the reactions that are occurring, such as NAD^+ degradation,

carbon-metal bonds, or NAD dimers. In addition, results suggest that this coenzyme can be stable under alkaline conditions, but not in acidic mediums. Adding a buffer to our experiments, such as PIPES, could help to maintain a high pH after adding salts and during the reaction. Screening NAD^+'s stability with other buffers that can support a more alkaline environment, also of most interest for studying hydrothermal conditions. However, this preliminary experiment gave some clues on how NAD could have been involved in the first metabolisms. In the absence of enzymes and other organic electron carriers, at 10 bar (H_2), magnetite was able to catalyze the synthesis of NADH, up to 147.91 µM. The irreplaceable role of iron has already been discussed for hydrogen bifurcation and CO_2 reduction under hydrothermal conditions, and here we hypothesize about its importance in the later stages of metabolism evolution. As discussed, ferredoxin is not only involved in the acetyl-CoA pathway directly and through hydrogenase redox reactions, but is also part of NAD's redox pathways. Thus, studying NAD^+'s reduction through iron-sulfur minerals, which resemble ferredoxin's catalytic center, could lead to interesting findings as Preiner et al. already used Fe_3S_4 to effectively reduce CO_2[6]. Furthermore, this work suggests that magnesium can be fit as a hydride transfer mechanism for NAD^+ reduction, and opens space for further discussion on its role in the origin of life. Magnesium is found in abundance both in the ocean's water and the hearth's crust. Nowadays, because it is highly soluble, it is available to organism's consumption. On the cellular level, it is the second most common cation, vital for multiple metabolic functions[81]. Wherever life started, salts must have played its part, and magnesium was likely present. Other works have used multiple inorganic molecules to mediate the interconversion of NAD^+ and NADH[82,83], and composites of magnesium hydrides are being developed and studied for hydrogen storage as do metal ammine salts, subject to specific catalysis for hydride desorption[79,84]. Moreover, Guan et al. already used iron composites to catalyze the reduction of aqueous CO_2[29]. Such materials, which are being developed for fuel and industry, could be applied in a different field of science to deeper investigate the role of metals and salts in the origin of metabolism.

5. References

1. Preiner, M. *et al.* The future of origin of life research: Bridging decades-old divisions. *Life* **10**, 1–25 (2020).
2. Tashiro, T. *et al.* Early trace of life from 3.95 Ga sedimentary rocks in Labrador, Canada. *Nature* **549**, 516–518 (2017).
3. Fuchs, G. *Alternative pathways of carbon dioxide fixation: Insights into the early evolution of life? Annual Review of Microbiology* vol. 65 (2011).
4. Sojo, V., Herschy, B., Whicher, A., Camprubí, E. & Lane, N. The Origin of Life in Alkaline Hydrothermal Vents. *Astrobiology* **16**, 181–197 (2016).
5. Varma, S. J., Muchowska, K. B., Chatelain, P. & Moran, J. Native iron reduces CO2 to intermediates and end-products of the acetyl-CoA pathway. *Nat. Ecol. Evol.* **2**, 1019–1024 (2018).
6. Preiner, M. *et al.* A hydrogen-dependent geochemical analogue of primordial carbon and energy metabolism. *Nat. Ecol. Evol.* **4**, 534–542 (2020).
7. Kelley, D. S. *et al.* An off-axis hydrothermal vent field near the mid-atlantic ridge at 30° n. *Nature* **412**, 145–149 (2001).
8. Kimura, J.-I. & Kawabata, H. Geochemistry, Geophysics, Geosystems. *Geochemistry Geophys. Geosystems* **16**, 267–300 (2015).
9. Preiner, M. *et al.* Serpentinization: Connecting geochemistry, ancient metabolism and industrial hydrogenation. *Life* **8**, (2018).
10. Russell, M. J. & Hall, A. J. The emergence of life from iron monosulphide bubbles at a submarine hydrothermal redox and pH front. *J. Geol. Soc. London.* **154**, 377–402 (1997).
11. Martin, W. & Russell, M. J. On the origin of biochemistry at an alkaline hydrothermal vent. *Philos. Trans. R. Soc. B Biol. Sci.* **362**, 1887–1925 (2007).
12. Baaske, P. *et al.* Extreme accumulation of nucleotides in simulated hydrothermal pore systems. *Proc. Natl. Acad. Sci. U. S. A.* **104**, 9346–9351 (2007).
13. Ding, Y., Batista, B., Steinbock, O., Cartwright, J. H. E. & Cardoso, S. S. S. Wavy membranes and the growth rate of a planar chemical garden: Enhanced diffusion and bioenergetics. *Proc. Natl. Acad. Sci. U. S. A.* **113**, 9182–9186 (2016).
14. Solin, S. A. Clays and clay intercalation compounds: Properties and physical phenomena. *Annu. Rev. Mater. Sci.* **27**, 89–115 (1997).

15. Aboudi Mana, S. C., Hanafiah, M. M. & Chowdhury, A. J. K. Environmental characteristics of clay and clay-based minerals. *Geol. Ecol. Landscapes* **1**, 155–161 (2017).

16. Pérez-Ramírez, J., Christensen, C. H., Egeblad, K., Christensen, C. H. & Groen, J. C. Hierarchical zeolites: Enhanced utilisation of microporous crystals in catalysis by advances in materials design. *Chem. Soc. Rev.* **37**, 2530–2542 (2008).

17. Qu, H., Ma, Y., Li, B. & Wang, L. Hierarchical zeolites: synthesis, structural control, and catalytic applications. *Emergent Mater.* **3**, 225–245 (2020).

18. BYK Additives & Instruments. Laponite : performance additives. *LAPONITE Perform. Addit.* 22 (2014) doi:10.1016/S0958-1669(97)80008-0.

19. Berger, F., Ramírez-Hernández, M. H. & Ziegler, M. The new life of a centenarian: Signalling functions of NAD(P). *Trends Biochem. Sci.* **29**, 111–118 (2004).

20. Lin, H. Nicotinamide adenine dinucleotide: Beyond a redox coenzyme. *Org. Biomol. Chem.* **5**, 2541–2554 (2007).

21. Kaster, A. K., Moll, J., Parey, K. & Thauer, R. K. Coupling of ferredoxin and heterodisulfide reduction via electron bifurcation in hydrogenotrophic methanogenic archaea. *Proc. Natl. Acad. Sci. U. S. A.* **108**, 2981–2986 (2011).

22. Schut, G. J. & Adams, M. W. W. The iron-hydrogenase of Thermotoga maritima utilizes ferredoxin and NADH synergistically: A new perspective on anaerobic hydrogen production. *J. Bacteriol.* **191**, 4451–4457 (2009).

23. Baross, J. & Hoffman, S. Submarine hydrothermal vents and associated gradient environments as sites f o r the o r i g i n a n d e v o l u t i o n of life. **15**, 327–345 (1985).

24. Schrenk, M. O., Brazelton, W. J. & Lang, S. Q. Serpentinization, carbon, and deep life. *Rev. Mineral. Geochemistry* **75**, 575–606 (2013).

25. Martin, W., Baross, J., Kelley, D. & Russell, M. J. Hydrothermal vents and the origin of life. *Nat. Rev. Microbiol.* **6**, 805–814 (2008).

26. Martin, W. F. Hydrogen, metals, bifurcating electrons, and proton gradients: The early evolution of biological energy conservation. *FEBS Lett.* **586**, 485–493 (2012).

27. Martin, W. F. Carbon–Metal Bonds: Rare and Primordial in Metabolism. *Trends Biochem. Sci.* **44**, 807–818 (2019).

28. Horita, J., Berndt, M. E., Horital, J. & Berndt, M. E. Abiogenic Methane Formation and Isotopic Fractionation Under Hydrothermal Conditions Published by : American Association for the Advancement of Science Stable URL : http://www.jstor.org/stable/2898541 Linked

references are available on JSTOR for this arti. **285**, 1055–1057 (2017).

29. Guan, G. *et al.* Reduction of aqueous CO2 at ambient temperature using zero-valent iron-based composites. *Green Chem.* **5**, 630–634 (2003).

30. Preiner, M. *et al.* Catalysts, autocatalysis and the origin of metabolism. *Interface Focus* **9**, (2019).

31. Ludwig, K. A., Kelley, D. S., Shen, C., Cheng, H. & Edwards, R. L. U/Th geochronology of carbonate chimneys at the Lost City hydrothermal field. *Am. Geophys. Union, Fall Meet.* abstract #V51B-1487 (2005).

32. Zahnle, K. J. Earth's earliest atmosphere. *Elements* **2**, 217–222 (2006).

33. Thauer, R. K. Hydrogenases and the global H2 cycle. *Eur. J. Inorg. Chem.* 919–921 (2011) doi:10.1002/ejic.201001255.

34. Can, M., Armstrong, F. A. & Ragsdale, S. W. Structure, function, and mechanism of the nickel metalloenzymes, CO dehydrogenase, and acetyl-CoA synthase. *Chem. Rev.* **114**, 4149–4174 (2014).

35. Wagner, T., Ermler, U. & Shima, S. The methanogenic CO2 reducing-and-fixing enzyme is bifunctional and contains 46 [4Fe-4S] clusters. *Science (80-.).* **354**, 114–117 (2016).

36. Herschy, B. *et al.* An Origin-of-Life Reactor to Simulate Alkaline Hydrothermal Vents. *J. Mol. Evol.* **79**, 213–227 (2014).

37. Brigatti, M. F., Malferrari, D., Laurora, A. & Elmi, C. Structure and mineralogy of layer silicates. *Layer. Miner. Struct. their Appl. Adv. Technol.* 1–71 (2012) doi:10.1180/emu-notes.11.1.

38. Číčel, B. & Komadel, P. Structural Formulae of Layer Silicates. *Quant. Methods Soil Mineral.* 114–136 (2015) doi:10.2136/1994.quantitativemethods.c4.

39. Savic, I. M., Stojiljkovic, S., Savic, I. & Gajic, D. Industrial application of clays and clay minerals. *Clays Clay Miner. Geol. Orig. Mech. Prop. Ind. Appl.* 379–402 (2014).

40. Kärger, J. & Freude, D. Mass Transfer in Micro- and Mesoporous Materials. *Chemie-Ingenieur-Technik* **73**, 1517–1527 (2001).

41. Verboekend, D., Mitchell, S. & Pérez-Ramírez, J. Hierarchical zeolites overcome all obstacles: Next stop industrial implementation. *Chimia (Aarau).* **67**, 327–332 (2013).

42. Selvam, T., Inayat, A. & Schwieger, W. Reactivity and applications of layered silicates and layered double hydroxides. *Dalt. Trans.* **43**, 10365–10387 (2014).

43. Kroon, M., Vos, W. L. & Wegdam, G. H. Structure and formation of a gel of colloidal disks. *Phys. Rev. E - Stat. Physics, Plasmas, Fluids, Relat. Interdiscip. Top.* **57**, 1962–1970 (1998).

44. Agoda-Tandjawa, G., Dieudé-Fauvel, E. & Baudez, J. C. Water dynamics and time-dependent structural changes of aqueous dispersions of Laponite: Linking water activity and rheology. *Appl. Clay Sci.* **132**–**133**, 528–534 (2016).

45. Zhu, X. & Tan, X. Metalloproteins/metalloenzymes for the synthesis of acetyl-CoA in the Wood-Ljungdahl pathway. *Sci. China, Ser. B Chem.* **52**, 2071–2082 (2009).

46. Goldford, J. E. & Segrè, D. Modern views of ancient metabolic networks. *Curr. Opin. Syst. Biol.* **8**, 117–124 (2018).

47. Peters, J. W., Miller, A. F., Jones, A. K., King, P. W. & Adams, M. W. W. Electron bifurcation. *Curr. Opin. Chem. Biol.* **31**, 146–152 (2016).

48. Buckel, W. & Thauer, R. K. Flavin-based electron bifurcation, ferredoxin, flavodoxin, and anaerobic respiration with protons (Ech) or NAD+ (Rnf) as electron acceptors: A historical review. *Front. Microbiol.* **9**, (2018).

49. Arnon, D. I. Ferredoxin and photosynthesis. *Science (80-.).* **149**, 1460–1469 (1965).

50. Xavier, J. C., Hordijk, W., Kauffman, S., Steel, M. & Martin, W. F. Autocatalytic chemical networks at the origin of metabolism. *Proc. R. Soc. B Biol. Sci.* **287**, (2020).

51. Eck, R. V. & Dayhoff, M. O. Evolution of the structure of ferredoxin based on living relics of primitive amino acid sequences. *Science (80-.).* **152**, 363–366 (1966).

52. Camprubi, E., Jordan, S. F., Vasiliadou, R. & Lane, N. Iron catalysis at the origin of life. *IUBMB Life* **69**, 373–381 (2017).

53. Rover, L. *et al.* Study of NADH stability using ultraviolet-visible spectrophotometric analysis and factorial design. *Anal. Biochem.* **260**, 50–55 (1998).

54. Hofmann, D., Wirtz, A., Santiago-Schübel, B., Disko, U. & Pohl, M. Structure elucidation of the thermal degradation products of the nucleotide cofactors NADH and NADPH by nano-ESI-FTICR-MS and HPLC-MS. *Anal. Bioanal. Chem.* **398**, 2803–2811 (2010).

55. ANDERSON, B. M. & ANDERSON, C. D. The effect of buffers on nicotinamide adenine dinucleotide hydrolysis. *J. Biol. Chem.* **238**, 1475–1478 (1963).

56. Wu, J. T., Wu, L. H. & Knight, J. A. Stabilityof NADPH: Effectof VariousFactorson the Kineticsof Degradation Materials and Methods. *Clin. Chem. Clin. Chem.* **32232**, 314–319 (1986).

57. Muchowska, K. B. *et al.* Metals promote sequences of the reverse Krebs cycle. *Nat. Ecol. Evol.*

1, 1716–1721 (2017).

58. Caldeira, K. & Wickett, M. E. Anthropogenic carbon and ocean pH. *Nature* **425**, 365 (2003).

59. Ng, E. P. & Mintova, S. Nanoporous materials with enhanced hydrophilicity and high water sorption capacity. *Microporous Mesoporous Mater.* **114**, 1–26 (2008).

60. Chua, H. T., Ng, K. C., Chakraborty, A., Oo, N. M. & Othman, M. A. Adsorption characteristics of silica gel + water systems. *J. Chem. Eng. Data* **47**, 1177–1181 (2002).

61. Gordeeva, L. G., Glaznev, I. S., Savchenko, E. V., Malakhov, V. V. & Aristov, Y. I. Impact of phase composition on water adsorption on inorganic hybrids 'salt/silica'. *J. Colloid Interface Sci.* **301**, 685–691 (2006).

62. Gordeeva, L. G. Selective water sorbents for multiple applications, 5. LiBr confined in mesopores of silica gel: Sorption properties. *React. Kinet. Catal. Lett.* **63**, 81–88 (1998).

63. Wambach, J., Illing, G. & Freund, H. J. CO2 activation and reaction with hydrogen on Ni(110): formate formation. *Chem. Phys. Lett.* **184**, 239–244 (1991).

64. He, C. S., Gong, L., Zhang, J., He, P. P. & Mu, Y. Highly selective hydrogenation of CO2 into formic acid on a nano-Ni catalyst at ambient temperature: Process, mechanisms and catalyst stability. *J. CO2 Util.* **19**, 157–164 (2017).

65. Blyholder, G., Shihabi, D., Wyatt, W. V. & Bartlett, R. Adsorption and interaction of C2H4, H2, CO, and organic acids on Fe, Co, and Ni. *J. Catal.* **43**, 122–130 (1976).

66. Li, L.-F., Ljungdahl, L. & Wood, H. G. Incorporation of C14 From Carbon Dioxide into Sugar Phosphates, Carboxylic Acids, and Amino Acids by Clostridium thermoaceticum. *J. Bacteriol.* **89**, 1055–1064 (1966).

67. Li, L.-F., Ljungdahl, L. & Wood, H. G. Properties of Nicotinamide Adenine Dinucleotide Phosphate-Dependent Formate Dehydrogenase from Clostridium thermoaceticum. *J. Bacteriol.* **92**, 405–412 (1966).

68. Eickenbusch, P. *et al.* Origin of short-chain organic acids in serpentinite mud volcanoes of the Mariana convergent margin. *Front. Microbiol.* **10**, 1–21 (2019).

69. Schuchmann, K. & Müller, V. Direct and reversible hydrogenation of CO2to formate by a bacterial carbon dioxide reductase. *Science (80-.).* **342**, 1382–1385 (2013).

70. McCollom, T. M. & Seewald, J. S. A reassessment of the potential for reduction of dissolved CO2 to hydrocarbons during serpentinization of olivine. *Geochim. Cosmochim. Acta* **65**, 3769–3778 (2001).

71. Bar-Even, A., Flamholz, A., Noor, E. & Milo, R. Thermodynamic constraints shape the

structure of carbon fixation pathways. *Biochim. Biophys. Acta - Bioenerg.* **1817**, 1646–1659 (2012).

72. Cody, G. D. *et al.* Primordial carbonylated iron-sulfur compounds and the synthesis of pyruvate. *Science (80-.).* **289**, 1337–1339 (2000).

73. Spectra, I., Molecules, F. O. R. & Ions, P. 10 . 2 : SPECTROSCOPY BASED ON ABSORPTION Example : Methane. 2–9 https://chem.libretexts.org/@go/page/70699%0D (2019).

74. Wiebe, R. & Gaddy, V. L. The Solubility of Hydrogen in Water at 0, 50, 75 and 100° from 25 to 1000 Atmospheres. *J. Am. Chem. Soc.* **56**, 76–79 (1934).

75. Varin, R. A., Czujko, T., Chiu, C., Pulz, R. & Wronski, Z. S. Synthesis of nanocomposite hydrides for solid-state hydrogen storage by controlled mechanical milling techniques. *J. Alloys Compd.* **483**, 252–255 (2009).

76. Vajo, J. J., Mertens, F., Ahn, C. C., Bowman, R. C. & Fultz, B. Altering hydrogen storage properties by hydride destabilization through alloy formation: LiH and MgH 2 destabilized with Si. *J. Phys. Chem. B* **108**, 13977–13983 (2004).

77. Ivanov, E., Konstanchuk, I., Stepanov, A. & Boldyrev, V. Magnesium mechanical alloys for hydrogen storage. *J. Less-Common Met.* **131**, 25–29 (1987).

78. Webb, C. J. A review of catalyst-enhanced magnesium hydride as a hydrogen storage material. *J. Phys. Chem. Solids* **84**, 96–106 (2015).

79. Varin, R. A., Zaranski, Z., Czujko, T., Polanski, M. & Wronski, Z. S. The composites of magnesium hydride and iron-titanium intermetallic. *Int. J. Hydrogen Energy* **36**, 1177–1183 (2011).

80. Cassells, J. M. & Halling, P. J. Effect of thermodynamic water activity on thermolysin-catalysed peptide synthesis in organic two-phase systems. *Enzyme Microb. Technol.* **10**, 486–491 (1988).

81. Jahnen-Dechent, W. & Ketteler, M. Magnesium basics. *CKJ Clin. Kidney J.* **5**, (2012).

82. Bunting, J. W. Merged mechanisms for hydride transfer from 1,4-dihydronicotinamides. *Bioorg. Chem.* **19**, 456–491 (1991).

83. Roberts, M. G., Ostovic, D. & Kreevoy, M. M. Hydride Transfer between. *Most* 257–265 (1982).

84. Sørensen, R. Z. *et al.* Indirect, reversible high-density hydrogen storage in compact metal ammine salts. *J. Am. Chem. Soc.* **130**, 8660–8668 (2008).

6. Appendix A

Appendix A. 1 Mass characterization of each of the six different types of samples for ZeoLap

Standard ZeoLapS			
	Mass (mg)	Relative percentage to ZeoLap	Weight concentration (% w/w)
ZeoLap mix	333,33	100,00	10,00
Ultra-pure water	3000		90,00
Total	3333,33		100,00

Standard ZeoLapS with Magnetite			
	Mass (mg)	Relative percentage to ZeoLap	Weight concentration (% w/w)
Magnetite (Fe3O4)	231,50	69,45	6,49
ZeoLap Mix	333,33	100,00	9,35
Ultra-pure water	3000		84,16
Total	3564,83		100,00

Standard ZeoLapS with Nickel			
	Mass (mg)	Relative percentage to ZeoLap (%)	Weight concentration (% w/w)
Nickel	177,00	53,10	5,04
ZeoLap Mix	333,33	100,00	9,50
Ultra-pure water	3000		85,46
Total	3510,33		100,00

Standard WaterS		
	Mass (mg)	Weight concentration (% w/w)
Ultra-pure water	3000,00	100,00
Total	3000	100,00

Standard WaterS with magnetite		
	Mass (mg)	Weight concentration (% w/w)
Fe_3O_4	231,50	7,16
Ultra-pure water	3000,00	92,84
Total	3231,5	100,00

	Mass (mg)	Weight concentration (% w/w)
Nickel	177,00	5,57
Ultra-pure water	3000,00	94,43
Total	3177	100,00

Appendix A. 2 HPLC essay on four contaminants relative to the percentage of Laonite-EP in the ZeoLap mixture and the amount of time it was heated and stirred on a magnetic heating mantle. All contaminations show a direct correlation with the two parameters tested, except for oxaloacetic acid.

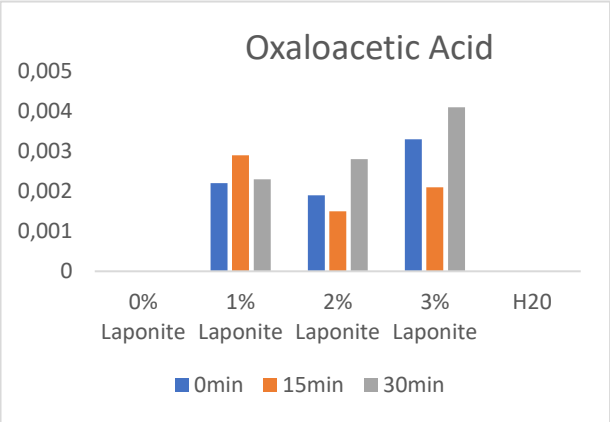

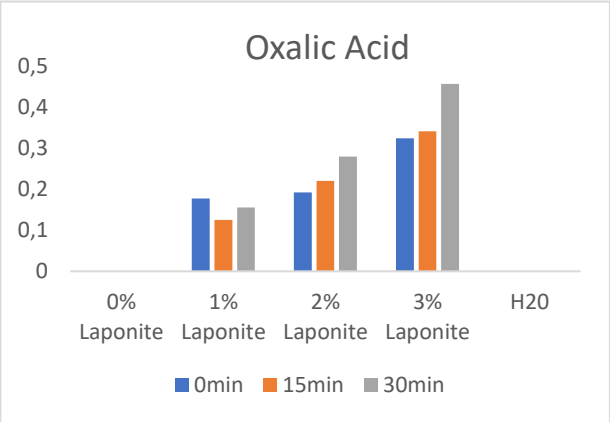

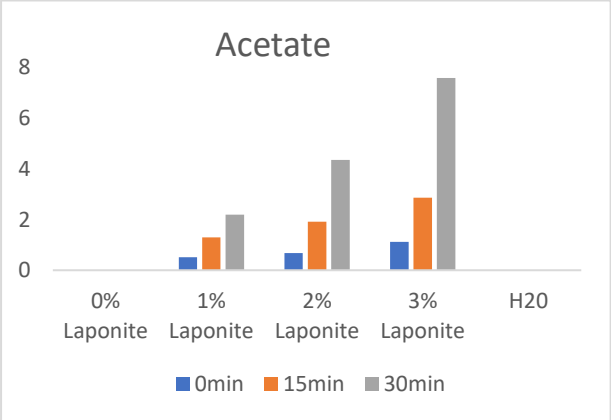

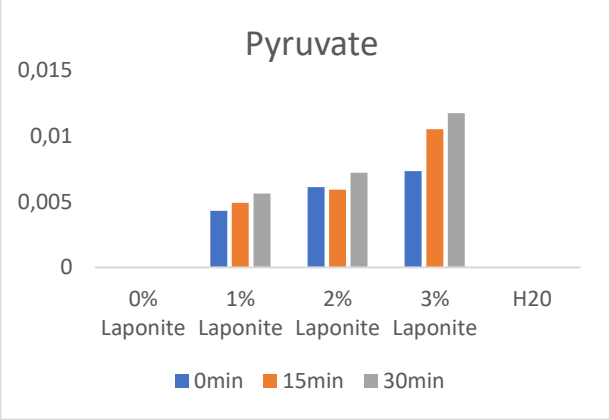

Appendix A. 3 H-NMR analysis controls for water samples.

	Concentration (mM)				
Gas phase	Formate	Methanol	Pyruvate	Acetate	Ethanol
Arg	0,0025	0,0005	0,0000	0,0020	0,0051
Arg+Ni	0,0038	0,0005	0,0000	0,0037	0,0071
Arg+Mag	0,0074	0,0006	0,0000	0,0255	0,0115
H2+Arg	0,0057	0,0022	0,0000	0,0048	0,0065
H2+Arg+Ni	0,0063	0,0023	0,0000	0,0072	0,0068
H2+Arg+Mag	0,0203	0,0020	0,0003	0,0200	0,0095

Appendix A. 5 H-NMR analysis controls for ZeoLapS

	Concentration (mM)				
Gas phase	Formate	Methanol	Pyruvate	Acetate	Ethanol
Arg	0,0031	0,0005	0,0000	0,0023	0,0063
Arg+Ni	0,0198	0,0005	0,0000	0,0028	0,0078
Arg+Mag	0,0108	0,0009	0,0002	0,0257	0,0117
H2+Arg	0,0047	0,0270	0,0005	0,0057	0,0106
H2+Arg+Ni	0,0091	0,0235	0,0000	0,0065	0,0068
H2+Arg+Mag	0,0175	0,0231	0,0008	0,0313	0,0084

Appendix A. 4 Pyruvate, acetate and ethanol as a product of CO_2 reduction compared between waterS, KOHS and ZeoLapS in mM.

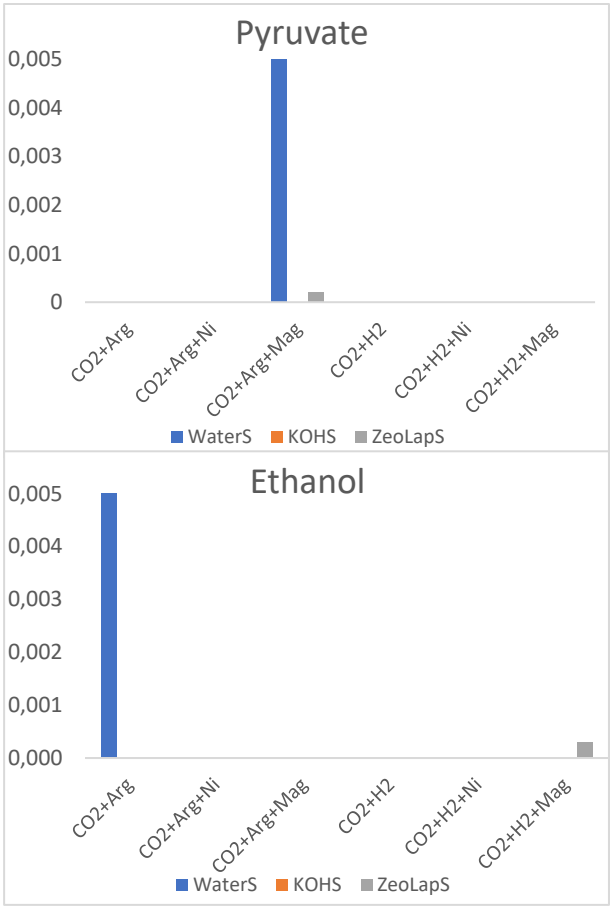

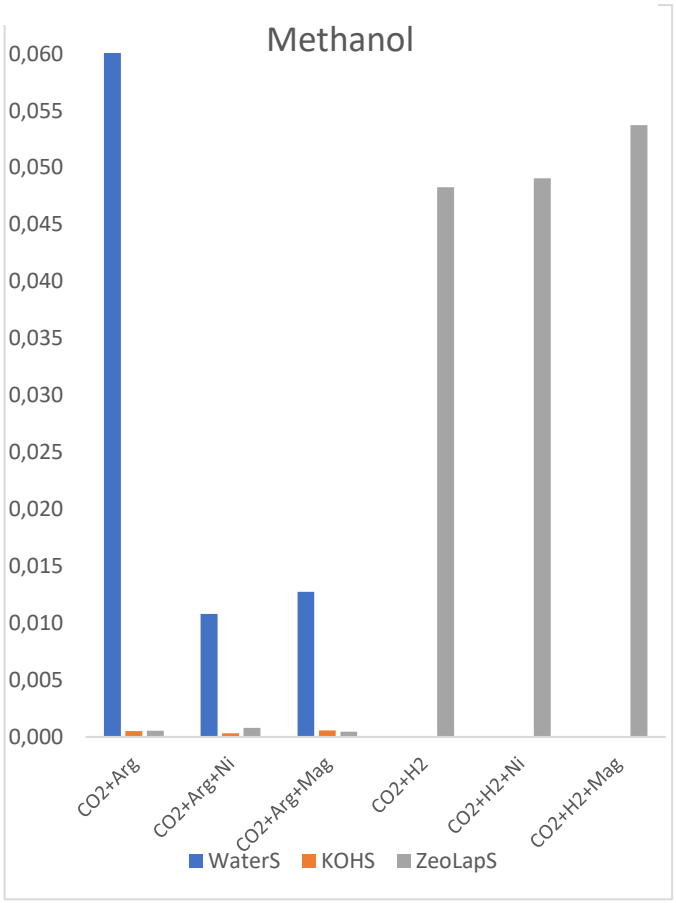

7. Appendix B

Appendix B. 1 H-NMR analysis standards provided by the laboratory

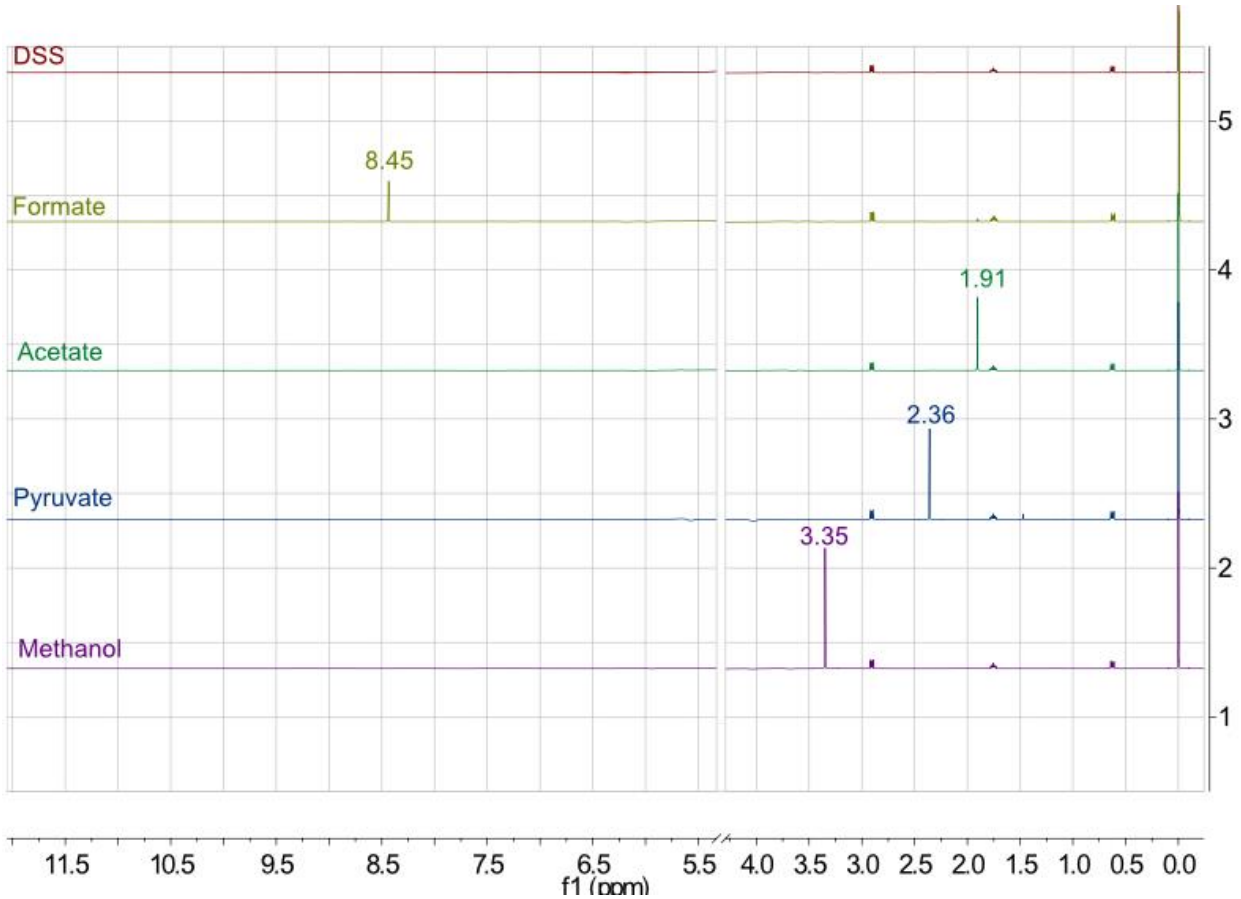

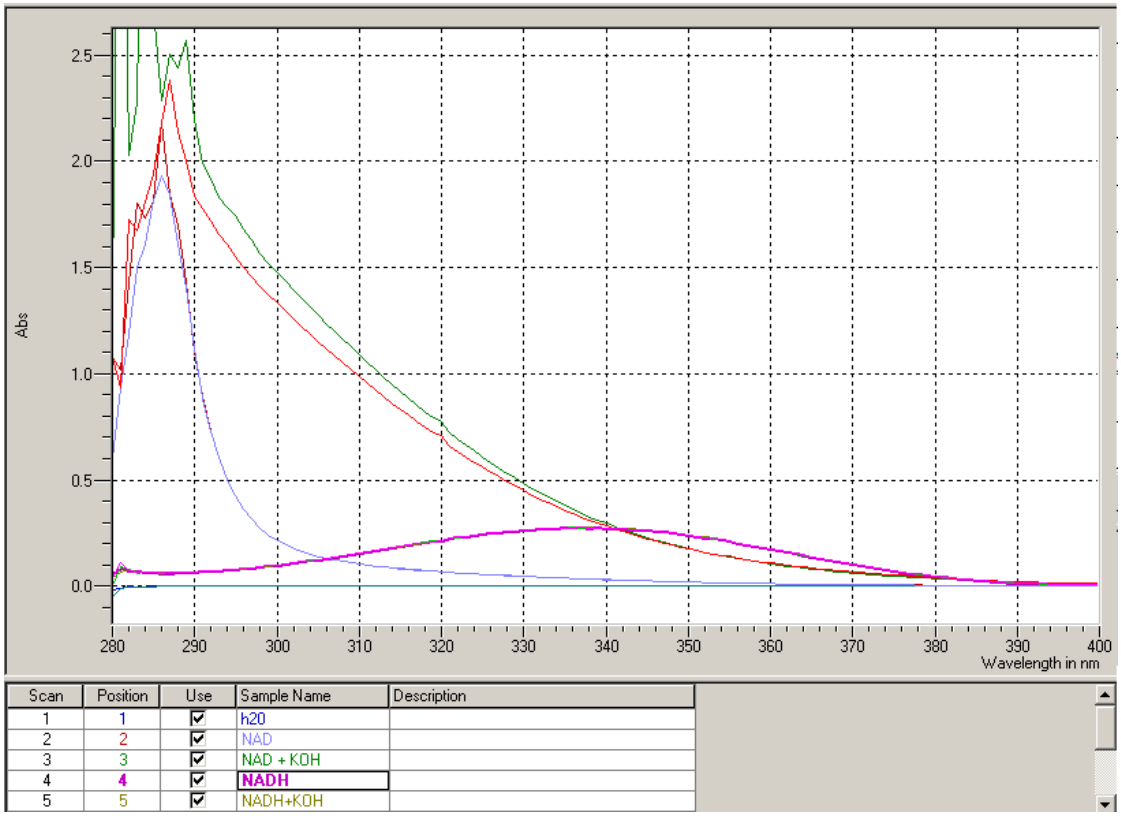

Scan	Position	Use	Sample Name	Description
1	1	☑	h20	
2	2	☑	NAD	
3	3	☑	NAD + KOH	
4	4	☑	NADH	
5	5	☑	NADH+KOH	

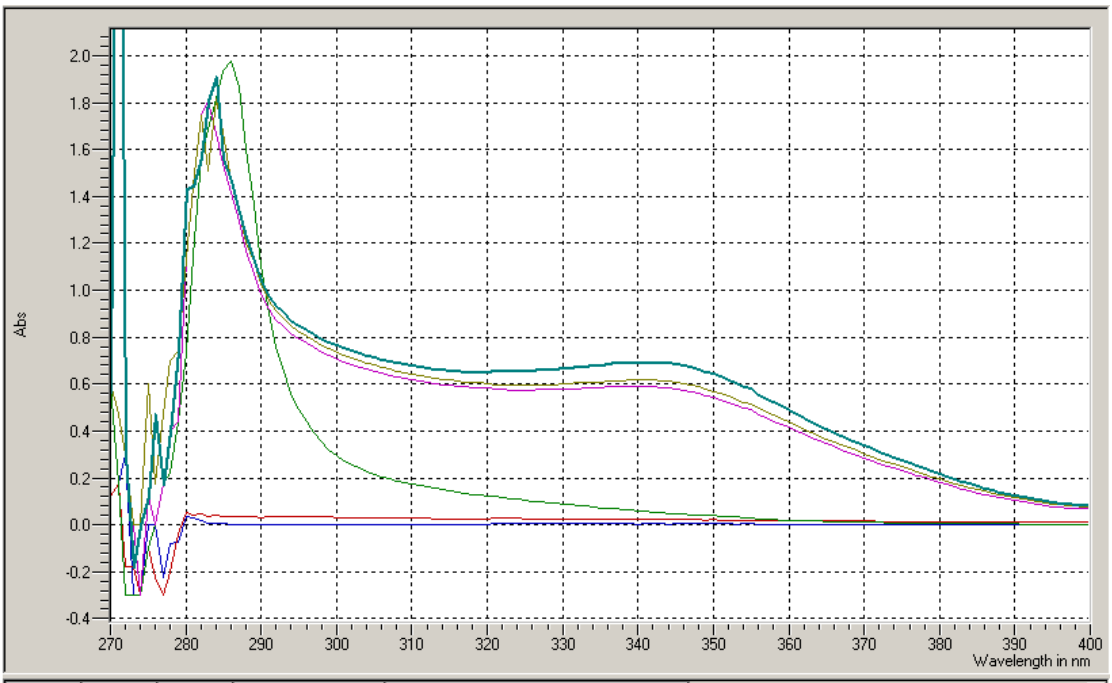

Scan	Position	Use	Sample Name	Description
2	2	☑	nad pre	
3	3	☑	fe	
4	4	☑	fe nad	
5	5	☑	fe nad	
6	6	☑	fe nad	

Appendix B. 2 NAD absorbance spectra under different conditions (270 nm – 400 nm). On the upper image, there are the spectra collected from solutions with NAD (3 mM) or NADH (0.05 mM), with and without KOH. On the bottom image, there are the spectra collected from solutions with NAD (3 mM) and triplicates with NAD (3 mM) and magnetite (Fe_3O_4). For the triplicates, the supernatant was collected, and the precipitated (magnetite) discarded.

8. Appendix C

Appendix C. 1 pH values of 10 mM concentrated solutions and water, with and without KOH. All samples were prepared with a previously made batch of alkaline water (pH = 10.2)

pH Controls	Before Reaction	10 bar Ar
H2O	8,75	9,76
H2O+10µl (of 0.5 mM KOH)	8,86	11,76
H2O+10µl (of 1 mM KOH)	8,73	12,08
MgCl2	6,77	-
FeCl2	3,36	-
FeCl2+10µl (of 1 mM KOH)	6,06	-